International Journal of Thermal Sciences 204 (2024) 109222

Contents lists available at ScienceDirect

International Journal of Thermal Sciences

journal homepage: www.elsevier.com/locate/ijts

On the network of thermal resistances embodying the response of geothermal boreholes to creeping groundwater flows

Javier Rico, Miguel Hermanns *

Departamento de Mecánica de Fluidos y Propulsión Aeroespacial, Escuela Técnica Superior de Ingeniería Aeronáutica y del Espacio, Universidad Politécnica de Madrid, Plaza Cardenal Cisneros 3, E-28040 Madrid, Spain

ARTICLE INFO

Keywords:
Geothermal boreholes
Groundwater flows
Thermal response
Low Peclet number
Thermal resistances
Apparent ground temperature

ABSTRACT

Aquifers are known to enhance the heat exchange between geothermal boreholes and the ground. To accurately assess this enhancement, theoretical models for the thermal interaction of geothermal boreholes with groundwater flows are necessary. Such models already exist in the literature but rely on ideas and methodologies intended for purely conductive grounds. Despite their satisfactory performance, the lack of mathematical rigor limits their capabilities and future development. The present work aims to overcome these limitations by deriving a mathematically rigorous and physically sound model for the case of creeping groundwater flows. This allows to evaluate, for the first time, the conceptual merits and limitations of the current state of the art and to envision ways of improving it.

1. Introduction

Mankind has embarked on a large-scale decarbonization of all human activities to counteract climate change. The European Union, for instance, aims to achieve net-zero CO_2 emissions by 2050 [1]. To accomplish this herculean task, activities with the highest potential for savings need to be addressed first. Since heating, ventilation, and air conditioning (HVAC) of buildings represent almost 23% of global energy consumption [2], replacing coal, fuel, and gas boilers with efficient, electricity-driven systems has become a top priority.

HVAC systems that rely on low-temperature geothermal energy represent an attractive solution to the aforementioned challenge. A geothermal HVAC system consists of an electricity-driven water-to-water heat pump connected to a geothermal heat exchanger composed of vertical boreholes. As shown in Fig. 1, each borehole is equipped with several pipes, forming coaxial or U-shaped probes, through which a heat-carrying liquid flows and exchanges heat with the surrounding ground. The space between pipes and ground is often filled with impermeable grout to prevent the cross-contamination of aquifers.

The correct design and sizing of geothermal heat exchangers ensures that the prescribed efficiency of the HVAC system is met throughout the building's lifetime, typically around 100 years. This requires long-term predictions of the thermal response of the boreholes and the surrounding ground during the design stages of the installation. Unfortunately, these forecasts cannot be obtained from detailed numerical simulations of the underlying heat transfer problem due to their excessive computational cost [3–12]. Instead, simplified models are needed that trade some flexibility and accuracy for improved computational speed, allowing for the design and sizing of geothermal heat exchangers to be accomplished within reasonable timeframes.

Numerous theoretical models for the thermal response of geothermal boreholes already exist in the literature. The first of these were introduced in the 1980s by researchers in Sweden [13–16]. By exploiting the significant disparity in time and length scales of the problem, they succeeded in deriving models for geothermal boreholes constructed in purely conductive grounds. These models proposed the use of networks of thermal resistances to represent the quasi-steady thermal response of the grout filling the boreholes and the ground close to the boreholes [16]. They also introduced the concept of borehole wall temperature, also known as apparent ground temperature [17], as a representation of the thermal state of the surrounding ground.

The validity and correctness of these two concepts were taken for granted at the time, and comparisons with experiments and numerical simulations supported this assumption [18,19]. However, the lack of a formal mathematical proof led to the exploration of alternative definitions for the network of thermal resistances and the borehole wall temperature in the quest for better results [20–22]. In 2014, a formal mathematical proof was finally given, nearly 30 years after the seminal work by Per Eskilson [15], providing clarity on the topic and allowing researchers to distinguish between mathematically correct and incorrect models [17].

Theoretical models that account for the presence of aquifers and the resulting convective heat transport in the ground also exist [23,24].

* Corresponding author.
E-mail addresses: j.rico@upm.es (J. Rico), miguel.hermanns@upm.es (M. Hermanns).

https://doi.org/10.1016/j.ijthermalsci.2024.109222
Received 7 March 2024; Received in revised form 24 May 2024; Accepted 14 June 2024
Available online 26 June 2024

Nomenclature

A, A, $\tilde{\mathrm{A}}$	Uniform temperature level imposed by the outer region onto the inner region [K], its non-dimensional counterpart [−], and its non-dimensional Laplace-transformed counterpart [−]
A_{0m}, A_{0m}, $\tilde{\mathrm{A}}_{0m}$	mth harmonic of the Fourier series expansion of T around the borehole [K], its non-dimensional counterpart [−], and its non-dimensional Laplace-transformed counterpart [−]
A_{0ma}	Weight of $\mathrm{q}_a/(2\pi\kappa)$ in A_{0m} [−]
α_b	Thermal diffusivity of grout [m^2/s]
α_g	Effective thermal diffusivity of ground [m^2/s]
B, B, $\tilde{\mathrm{B}}$	Uniform temperature level imposed by the outer region onto the inner region [K], its non-dimensional counterpart [−], and its non-dimensional Laplace-transformed counterpart [−]
$B_{0\ell}$	Integration constants in Θ_p [−]
C, C, $\tilde{\mathrm{C}}$	Coefficient specifying the temperature gradient imposed by the outer region onto the inner region [K], its non-dimensional counterpart [−], and its non-dimensional Laplace-transformed counterpart [−]
C_{in}	Weight of F_{in} in the multipole expansion of Θ [−]
C_{ina}	Subweight of $\mathrm{q}_a/(2\pi\kappa)$ in C_{in} [−]
$C_{in,\mathrm{c}}$, $C_{in,\bar{\mathrm{c}}}$	Subweights of C and of its complex conjugate $\overline{\mathrm{C}}$ in C_{in}, respectively [−]
COP	Coefficient of Performance [−]
d_j	Thickness of the wall of pipe j [m]
δ_{ij}	Kronecker's delta [−]
E_1	Exponential integral [−]
f	Non-dimensional fictitious heat injection rate per unit borehole length [−]
F_{in}	Multipole n centered at pipe i [−]
$\mathcal{F}_{injm}$, $\mathcal{F}'_{injm}$	mth harmonic of the Fourier series expansions of F_{in} and of its radial derivative, respectively, around pipe j or around the borehole ($j = 0$) [−]
$\mathcal{G}_{0m}$, $\mathcal{G}'_{0m}$	mth harmonic of the Fourier series expansions of Θ_g and of its radial derivative, respectively, around the borehole [−]
γ	Euler's constant [−]
h_j	Convective heat transfer coefficient of pipe j [W/(m^2K)]
H	Depth of borehole [m]
HVAC	Heating, Ventilation, and Air Conditioning
$\imath$	Imaginary unit [−]
k_b	Thermal conductivity of grout [W/(m K)]
k_g	Effective thermal conductivity of ground [W/(m K)]
k_j	Thermal conductivity of the wall of pipe j [W/(m K)]
κ	Ratio between the thermal conductivity of grout and the effective thermal conductivity of ground [−]
$\mathcal{L}$	Non-dimensional Laplace operator [−]
λ	Dummy non-dimensional integration variable [−]
N_p	Number of pipes in the borehole [−]
Pe	Peclet number of groundwater flow [−]
$\mathcal{P}_{jm}$, $\mathcal{P}'_{jm}$	mth harmonic of the Fourier series expansions of Θ_p and of its radial derivative, respectively, around pipe j or around the borehole ($j = 0$) [−]
$\mathcal{P}_{jma}$, $\mathcal{P}'_{jma}$	Weights of $\mathrm{q}_a/(2\pi\kappa)$ in $\mathcal{P}_{jm}$ and $\mathcal{P}'_{jm}$, respectively [−]
q, q, $\tilde{\mathrm{q}}$	Heat injection rate per unit borehole length [W/m], its non-dimensional counterpart [−], and its non-dimensional Laplace-transformed counterpart [−]
q_j, q_j, $\tilde{\mathrm{q}}_j$	Heat injection rate per unit pipe length of pipe j [W/m], its non-dimensional counterpart [−], and its non-dimensional Laplace-transformed counterpart [−]
q_c	Characteristic value for q and q_j [W/m]
r_b	Borehole radius [m]
r_j, ρ_j	Radial coordinate of the polar coordinate system centered at pipe j or at the borehole ($j = 0$) [m] and its non-dimensional counterpart [−]
r_{0j}, ρ_{0j}	Radial position of pipe j in the polar coordinate system centered at the borehole [m] and its nondimensional counterpart [−]
r_{pj}, ρ_{pj}	Radius of pipe j or of the borehole ($j = 0$) [m] and its non-dimensional counterpart [−]
$\mathrm{R}_{a,ij}$	Non-dimensional borehole's inner thermal resistances [−]
R_b	Non-dimensional borehole's outer thermal resistance [−]
R_{ij}	Non-dimensional thermal resistances of the borehole [−]
$\hat{R}_{ij}$, $\hat{\mathrm{R}}_{ij}$	Thermal resistances of the borehole [(m K)/W] and their non-dimensional counterparts [−]
$\hat{\mathrm{R}}_{ij}^{(0)}$, $\hat{\mathrm{R}}_{ij}^{(1)}$	Zeroth-order solution and first-order correction of the thermal resistances of the borehole, respectively [−]
R_{pj}, R_{pj}	Inner thermal resistance of pipe j [(m K)/W] and its non-dimensional counterpart [−]
s	Non-dimensional position in the complex-valued Laplace plane [−]
t, τ	Time [s] and its non-dimensional counterpart [−]
t_b	Characteristic transversal diffusion time [s]
t_c	Characteristic residence time of the groundwater stream in the vicinity of the borehole [s]
t_H	Characteristic longitudinal diffusion time [s]
t_q	Characteristic timescale of the variations in the heating and cooling needs of the building [s]
t_r	Characteristic residence time of the heat carrying liquid in the pipes [s]
T_∞	Unperturbed ground temperature [K]
T, Θ	Perturbed grout/ground temperature [K] and its non-dimensional counterpart [−]

T_a, Θ_a	Apparent ground temperature or weighted apparent ground temperature [K] and its non-dimensional counterpart [−]
T_{aj}, Θ_{aj}	Apparent ground temperature for pipe j [K] and its non-dimensional counterpart [−]
T_j, Θ_j	Temperature of the fluid in pipe j [K] and its non-dimensional counterpart [−]
θ_j	Angular coordinate of the polar coordinate system centered at pipe j or at the borehole ($j = 0$) [rad]
θ_{0j}	Angular position of pipe j in the polar coordinate system centered at the borehole [rad]
$\Theta^{(0)}$, $\Theta^{(1)}$	Zeroth-order solution and first-order correction of the grout/ground temperature, respectively [−]
$\Theta_{aj}^{(0)}$, $\Theta_{aj}^{(1)}$	Zeroth-order solution and first-order correction of the apparent ground temperature for pipe j, respectively [−]
$\Theta_{\text{ex}}^{(1)}$, $\Theta_{\text{en}}^{(1)}$	Exogenous and endogenous first-order corrections of the grout/ground temperature, respectively [−]
$\Theta_j^{(0)}$, $\Theta_j^{(1)}$	Zeroth-order solution and first-order correction of the temperature of the fluid in pipe j, respectively [−]
$\Theta_{j,\text{ex}}^{(1)}$, $\Theta_{j,\text{en}}^{(1)}$	Exogenous and endogenous first-order correction of the temperature of the fluid in pipe j, respectively [−]
Θ_g	Particular solution of the governing equation in the ground [−]
Θ_m	Non-dimensional weighted mean fluid temperature of the borehole [−]
Θ_p	Particular solution [−]
U_∞	Effective seepage velocity of the groundwater flow [m/s]
v_j	Secondary weighting coefficient of pipe j [−]
v_r, v_r	Radial component of the effective velocity of the groundwater flow [m/s] and its non-dimensional counterpart [−]
v_θ, v_θ	Azimuthal component of the effective velocity of the groundwater flow [m/s] and its non-dimensional counterpart [−]
V	Bulk velocity of the heat carrying liquid [m/s]
w_j	Primary weighting coefficient of pipe j [−]

These models replicate the methodology and ideas of those designed for purely conductive grounds. So, they use a network of thermal resistances to represent the quasi-steady thermal response of the grout filling the boreholes and the ground close to the boreholes [25,26], and they employ a borehole wall temperature, or apparent ground temperature, to describe the thermal state of the surrounding ground.

The validity and correctness of these two concepts, now in the context of groundwater flows, are again taken for granted in the literature, with comparisons to experiments and numerical simulations supporting this assumption [24]. However, without a formal mathematical proof, it is impossible to fully assess the merits and limits of the current state of the art and to envision mathematically sound ways of improving it.

The present work addresses the aforementioned lack of mathematical rigor by providing a formal proof for the case of creeping groundwater flows. In this flow regime, which forms the basis of most theoretical models available today, heat convection near the borehole is weak compared to heat conduction.

Three main conclusions are drawn from the presented proof. First, the quasi-steady thermal response of the grout filling the borehole and the ground near the borehole can also be represented by a network of thermal resistances when groundwater flows are present. Second, the structure of this network differs from the one employed in the literature. The same applies to the temperature representing the thermal state of the surrounding ground. Third, the identified inconsistencies in the state of the art do not affect the performance of existing models as long as creeping groundwater flows are considered.

The present work is organized as follows. Section 2 extensively discusses the thermal interaction of geothermal boreholes with groundwater flows. It begins by examining the state of the art and the findings of the present study, then formulates the governing equations for general groundwater flows, and subsequently particularizes them for the case of creeping groundwater flows. Next, Section 3 introduces a modified version of the enhanced multipole method to account for creeping groundwater flows. Following that, Section 4 solves the formulated problem using the modified enhanced multipole method. The obtained solutions are then exploited in Sections 5 and 6 to infer the structure of the network of thermal resistances and the appropriate temperature, or temperatures, to describe the thermal state of the ground surrounding the borehole. Subsequently, numerical examples are provided in Section 7. Finally, Section 8 presents the conclusions of the work.

2. Interaction of boreholes with aquifers

A geothermal borehole, like the one shown in Fig. 1, is a slender hole, of depth H and radius r_b, drilled vertically into the ground. It is equipped with several pipes forming one or more coaxial or U-shaped probes. A heat carrying liquid is then forced to flow through these pipes, with a bulk velocity V, to exchange heat with the surrounding ground.

The thermal response of a geothermal borehole is known to depend on five characteristic times [27]. Three of them are directly linked to the aforementioned characteristics of the borehole and to the effective thermal diffusivity of the ground α_g. These are the characteristic residence time $t_r \sim H/V$ of the heat carrying liquid in the pipes, the characteristic transversal diffusion time $t_b \sim r_b^2/\alpha_g$ in the ground, and the characteristic longitudinal diffusion time $t_H \sim H^2/\alpha_g$, also in the ground [17]. Considering realistic values for the involved parameters, the sequence of characteristic times is $t_r \ll t_b \ll t_H$ [17].

The fourth characteristic time, associated with the presence of an aquifer, is the characteristic residence time $t_c \sim r_b/U_\infty$ representing the time the groundwater stream spends near the borehole [27]. Here, U_∞ denotes the effective seepage velocity of the stream [26,28,29]. The present work focuses on creeping groundwater flows for which $t_b \ll t_c$ [27]. Hence, the extended sequence of characteristic times becomes $t_r \ll t_b \ll t_c \ll t_H$.

The fifth characteristic time, t_q, represents the timescale of variations in the heating and cooling requirements of the building. Given that these needs fluctuate on an hourly, daily, weekly, monthly, and yearly basis, t_q encompasses a broad spectrum of values ranging from minutes to decades [17]. This work focuses on the most relevant case of slowly varying heating/cooling demands for which $t_c \ll t_q \ll t_H$ [27]. Therefore, the complete sequence of characteristic times for the problem under consideration is

$$t_r \ll t_b \ll t_c \ll t_q \ll t_H.$$

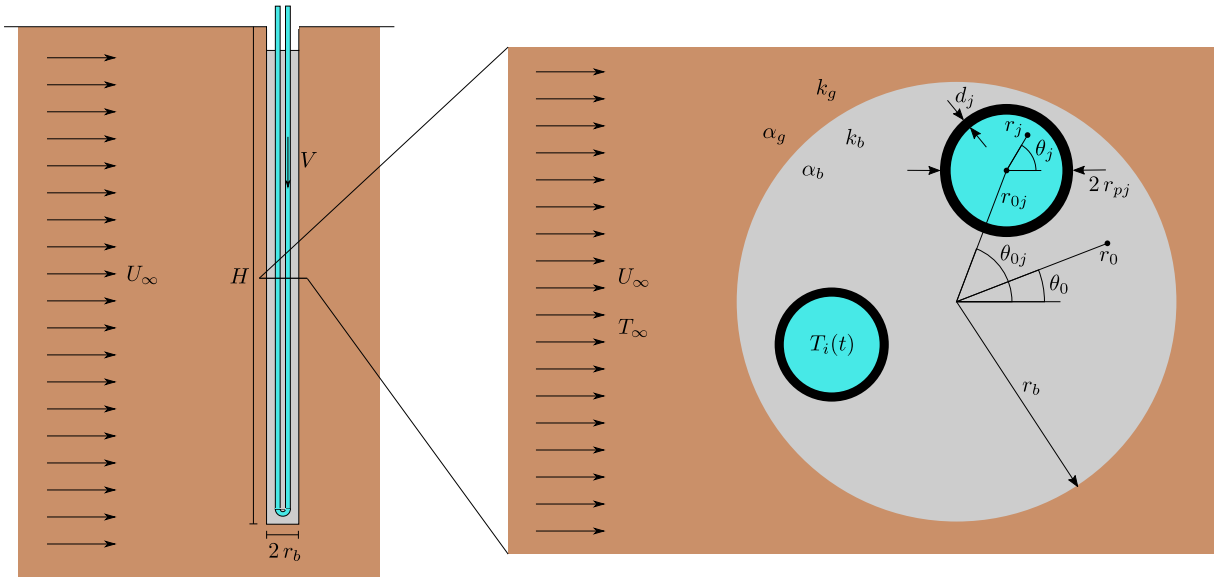

Fig. 1. Sketch of a typical geothermal borehole.

2.1. Negligible axial heat transfer

The extreme slenderness of geothermal boreholes allows for the simplification of the three-dimensional heat transfer problem in the ground. On one hand, heat conduction along the borehole is negligible compared to heat conduction in the radial direction, primarily due to t_b and t_q being significantly smaller than t_H [17]. On the other hand, aquifers predominantly flow perpendicular to the boreholes due to the small slopes of piezometric pressure levels in the ground.

The aforementioned simplifications enable the reinterpretation of the three-dimensional heat transfer problem as two-dimensional heat transfer problems formulated in planes perpendicular to the borehole, with coupling between these planes occurring solely through the convective transport of heat along the pipes [17,27]. Fig. 1 illustrates one such plane perpendicular to the borehole. This reinterpretation does not alter the potential dependence on depth of the thermal characteristics and state of the ground, aquifer, grout, etc., as each two-dimensional heat transfer problem is solved using values corresponding to the respective depths.

2.2. Two-region structure

The present work focuses on slowly-varying heat injection rates for which t_b is small compared to t_q [17,27]. This limit is extensively exploited in the literature for the development of theoretical models for the thermal response of geothermal boreholes [15,16,30–37].

In the limit of slowly-varying heat injection rates, a two-region structure emerges in each plane [17,27]. The inner region, situated at radial distances from the borehole comparable to the borehole radius, $r \sim r_b$, exhibits a quasi-steady thermal response of the grout filling the borehole and the ground located close to the borehole. Conversely, thermal inertia of the ground plays a fundamental role in the outer region, located farther away from the borehole, at radial distances of order $r \sim r_b\sqrt{t_q/t_b} \gg r_b$.

The described two-region structure has been addressed recently [17] using matched asymptotic expansion techniques [38]. These techniques solve each region separately and then interweave, or match, the resulting solutions at an intermediate distance from the borehole, situated between the two regions. In this context, the present work focuses solely on solving the inner region and its matching, as the outer region is well described and understood in existing literature [23,24,27].

The influence of aquifers in the inner region is determined by the Peclet number of the groundwater flow [27],

$$\mathrm{Pe} = \frac{r_b U_\infty}{\alpha_g}.$$

This non-dimensional number gauges the relative importance of heat convection compared to heat conduction in the energy conservation equation within the ground [39]. Two distinct cases are subsequently discussed to elucidate the objective of the present work and its findings.

2.2.1. Purely-conducting limit

In the absence of groundwater flows, heat transfer in the ground is solely driven by conduction, resulting in a Peclet number of zero for the problem. The exact solution to the quasi-steady inner region can then be obtained using the enhanced multipole method [40,41]. The key result is the following relationship between heat injection rates per unit pipe length $q_j(t)$, specified at the N_p pipes of the borehole, and resulting temperatures $T_i(t)$ of the liquid in the pipes:

$$\sum_{j=1}^{N_p} \hat{R}_{ij} q_j(t) = T_i(t) - T_a(t). \tag{1}$$

The thermal resistances $\hat{R}_{ij}$, which link the two quantities of interest in the preceding expression, depend on the geometry and thermal properties of the borehole, as well as the thermal conductivity of the ground. As provided by the enhanced multipole method, their values remain constant over time in the limit of slowly-varying heat injection rates [40].

The apparent ground temperature $T_a(t)$ represents the temperature at which the borehole perceives its surrounding ground [41]. It is a quantity imposed by the outer region onto the inner region that includes three phenomena: the unperturbed ground temperature T_∞, the thermal influence exerted by neighboring boreholes, and the thermal influence exerted by the borehole on itself [17,42].

2.2.2. Creeping groundwater flows

The heat transfer problem to be solved in the inner region changes with the presence of a groundwater stream in the ground, leading to an important question: Does a network of thermal resistances, similar to Eq. (1), still connect heat injection rates per unit pipe length $q_j(t)$ with fluid temperatures $T_i(t)$ in the pipes?

The present study addresses this specific question for the particular case of creeping groundwater flows, where the Peclet number is small

compared to unity. To find the answer, the asymptotic analysis of the thermal interaction of geothermal boreholes with creeping groundwater flows, recently conducted by the authors [27], is used as starting point. The solution to the inner region, previously obtained numerically [27], needs to be derived analytically instead to enable the correct identification and precise definition of thermal resistances and apparent ground temperatures. This task is accomplished in the present work by developing a modified version of the enhanced multipole method.

Anticipating the results of Sections 5 and 6, the exact solution to the inner region yields the following relationship between the heat injection rates per unit pipe length $q_j(t)$ and the fluid temperatures $T_i(t)$ in the pipes:

$$\sum_{j=1}^{N_p} \hat{R}_{ij} q_j(t) = T_i(t) - T_{ai}(t). \tag{2}$$

There are two differences compared to the purely-conducting case discussed before. Firstly, each pipe perceives the surrounding ground at a different apparent temperature $T_{ai}(t)$. This discrepancy arises from the asymmetry introduced by the convective heat transport in the outer region, which manifests as a temperature gradient imposed on the inner region. The thermal response of the inner region to this gradient results in distinct apparent ground temperatures for each pipe.

The second difference with the purely-conducting case is that thermal resistances $\hat{R}_{ij}$ now depend on the Peclet number of the groundwater flow. This stems directly from the convective heat transport near the borehole, even in the case of creeping groundwater flows under consideration.

2.3. State of the art

As emphasized in the preceding subsection, the presence of a groundwater stream alters the mathematical structure and the values of the network of thermal resistances that connect heat injection rates per unit pipe length $q_j(t)$ with fluid temperatures $T_i(t)$ in the pipes. This has significant implications for the current state of the art.

Numerous theoretical models exist in the literature for the thermal interaction of boreholes with aquifers. Most of these models explicitly [15,25,26,43–51] or implicitly [28,29,52–60] incorporate a network of thermal resistances to represent the quasi-steady thermal response of the grout filling the borehole and the ground close to the borehole. The adoption of this modeling approach is rooted in the successful utilization of such networks by theoretical models for the thermal response of geothermal boreholes constructed in purely conductive grounds.

All reviewed models adopt without changes the structure and values of the network of thermal resistances, Eq. (1), valid for purely conductive grounds. In the absence of mathematical proofs guiding researchers on how to proceed in a mathematically sound manner, the decision taken seems to be the most logical one. However, with the availability now of Eq. (2), derived from a mathematical proof valid for creeping groundwater flows, it is now possible for the first time to assess the strengths and limitations of the current state of the art.

Consequently, two conceptual errors are identified in the existing body of literature due to the differences discussed in the previous subsection. Firstly, current models for the thermal interaction of boreholes with aquifers overlook the influence of the aquifer on the thermal resistances. Secondly, they only consider one apparent ground temperature for all pipes. The examination of the practical implications of these two discrepancies is the focus of Section 7.

2.4. Formulation of inner problem

Consider the two-dimensional heat transfer problem represented in the right half of Fig. 1. The borehole, with a radius of r_b, is outfitted with N_p pipes and filled with impermeable grout, characterized by its thermal conductivity k_b and thermal diffusivity α_b, which differ from the effective thermal conductivity k_g and effective thermal diffusivity α_g of the ground, respectively.

Each pipe j is defined by its outer radius r_{pj}, wall thickness d_j, and thermal conductivity k_j. The position of pipe j within the borehole is determined by the coordinates (r_{0j}, θ_{0j}) of its center in the polar coordinate system (r_0, θ_0) centered at the borehole. The orientation of the coordinate system (r_0, θ_0) aligns such that $\theta_0 = 0°$ corresponds to the flow direction of the unperturbed groundwater stream.

The temperature T within the impermeable grout is governed by the following quasi-steady energy conservation equation, where heat conduction is the sole heat transfer mechanism:

$$0 = \frac{1}{r_0}\frac{\partial}{\partial r_0}\left(r_0 \frac{\partial T}{\partial r_0}\right) + \frac{1}{r_0^2}\frac{\partial^2 T}{\partial \theta_0^2}.$$

Conversely, the quasi-steady energy conservation equation governing the temperature T in the ground also includes heat convection [27],

$$v_r \frac{\partial T}{\partial r_0} + \frac{v_\theta}{r_0}\frac{\partial T}{\partial \theta_0} = \alpha_g \left[\frac{1}{r_0}\frac{\partial}{\partial r_0}\left(r_0 \frac{\partial T}{\partial r_0}\right) + \frac{1}{r_0^2}\frac{\partial^2 T}{\partial \theta_0^2}\right],$$

with the effective velocity components (v_r, v_θ) of the groundwater flow given by the following expressions [27]:

$$v_r = \; U_\infty \left(1 - \frac{r_b^2}{r_0^2}\right)\cos(\theta_0),$$

$$v_\theta = -U_\infty \left(1 + \frac{r_b^2}{r_0^2}\right)\sin(\theta_0).$$

At the borehole wall, where $r_0 = r_b$, continuity in temperatures and normal heat fluxes must be ensured so that

$$T\Big|_{r_0=r_b^-} = T\Big|_{r_0=r_b^+} \qquad \text{and} \qquad -k_b \frac{\partial T}{\partial r_0}\Big|_{r_0=r_b^-} = -k_g \frac{\partial T}{\partial r_0}\Big|_{r_0=r_b^+}.$$

Next, boundary conditions at the N_p pipes inside the borehole must be specified, for which a polar coordinate system (r_j, θ_j) centered at each pipe j is introduced for convenience. A prescribed heat injection rate per unit pipe length $q_j(t)$ is then specified at each pipe j using the following expression:

$$q_j(t) = \int_{-\pi}^{\pi} -k_b \frac{\partial T}{\partial r_j}\Big|_{r_j=r_{pj}} r_{pj}\, \mathrm{d}\theta_j.$$

This condition, however, is not mathematically sufficient, so an additional condition is enforced at each point on the outer surface of pipe j [17]:

$$-k_b r_{pj} \frac{\partial T}{\partial r_j}\Big|_{r_j=r_{pj}} = \frac{T_j(t) - T\big|_{r_j=r_{pj}}}{R_{pj}},$$

with the bulk temperature $T_j(t)$ of the fluid in pipe j conveniently set to ensure the prescribed heat injection rate per unit pipe length $q_j(t)$ is satisfied at all times [27]:

$$T_j(t) = \frac{R_{pj}}{2\pi} q_j(t) + \frac{1}{2\pi}\int_{-\pi}^{\pi} T\Big|_{r_j=r_{pj}} \mathrm{d}\theta_j.$$

The pipe's inner thermal resistance R_{pj}, appearing in the previous two expressions, accounts for heat conduction within the pipe wall and for the convective transport of heat within the fluid. Modeling the latter phenomenon using a convective heat transfer coefficient h_j leads to the following expression for R_{pj} [17]:

$$R_{pj} = \frac{1}{(r_{pj} - d_j)h_j} + \frac{1}{k_j}\ln\left(\frac{r_{pj}}{r_{pj} - d_j}\right).$$

2.4.1. Matching with outer problem

The problem formulated thus far requires one additional boundary condition to be enforced far from the borehole. However, that boundary condition cannot be the unperturbed ground temperature T_∞ because

the unsteady outer region lies in between, altering the borehole's perception of its surrounding ground [27].

The condition to enforce far from the borehole must therefore be the compatibility between solutions obtained for the inner and outer regions. This is achieved through the asymptotic matching of the two solutions at a distance located between the two regions [38].

In the absence of aquifers, which corresponds to a zero Peclet number, the matching condition to enforce at the outer boundary of the inner region is well known and was mathematically proven by the second author in 2014 [17]:

$$r_0 \to \infty : \; T \to T_a(t) - \frac{q(t)}{2\pi k_g} \ln\left(\frac{r_0}{r_b}\right), \tag{3}$$

with the heat injection rate per unit borehole length $q(t)$ representing the total amount of heat exchanged between the borehole and ground per unit time and unit borehole length:

$$q(t) = \sum_{j=1}^{N_p} q_j(t).$$

The first term in Eq. (3) is the apparent ground temperature, which also appears in the network of thermal resistances given in Eq. (1). This term represents a uniform temperature level imposed by the outer region onto the inner region [17], with its value derived from the solution to the outer region. The second term in Eq. (3) is imposed by the inner region onto the outer region. It is an inherent part of the solution to the inner region and is ultimately responsible for the thermal reaction of the ground located in the outer region.

The corresponding matching condition when groundwater flows are present differs from Eq. (3). For creeping groundwater flows, where Peclet numbers are small compared to unity, the authors have mathematically established the new matching condition using two distinct approaches.

In the first approach, they employed the matching condition resulting from the asymptotic analysis of the thermal interaction of geothermal boreholes with creeping groundwater flows [27]. In the second approach, they utilized the asymptotic analysis of the thermal interaction of geothermal boreholes with strong groundwater flows, where the Peclet number is of order unity [61]. In this case, the proposed matching condition is derived by analyzing the behavior of the outer solution near the borehole when the Peclet number is made small compared to unity.

Both approaches yield the same expression for the matching condition, which can be extended to incorporate the thermal influence from neighboring boreholes. The resulting expression, wherein $\imath = \sqrt{-1}$, is

$$\begin{aligned} r_0 \to \infty : \; T \to A(t) &- \frac{q(t)}{2\pi k_g} \ln\left(\frac{r_0}{r_b}\right) \\ &+ \mathrm{Pe}\left[B(t) + C(t)\frac{r_0}{r_b}\mathrm{e}^{+\imath\theta_0} + \overline{C}(t)\frac{r_0}{r_b}\mathrm{e}^{-\imath\theta_0}\right] \\ &+ \mathrm{Pe}\left[\frac{A_{0(+1)}(t) + A_{0(-1)}(t)}{2} - \frac{q(t)}{4\pi k_g}\frac{r_0}{r_b}\cos(\theta_0)\right]\ln\left(\frac{r_0}{r_b}\right). \end{aligned} \tag{4}$$

The uniform temperature level imposed by the outer region onto the inner region is now represented by $A(t)$ and $B(t)$. Its value encompasses not only the unperturbed ground temperature and the thermal self-influence of the borehole but also the effects of the groundwater flow and the influence of neighboring boreholes.

The pair $C(t)$ and $\overline{C}(t)$ represents a temperature gradient also imposed by the outer region onto the inner region. These quantities are complex conjugates that specify both the intensity and spatial direction of the temperature gradient. This direction does not necessarily coincide with the groundwater flow direction when the borehole is influenced by the thermal wakes of upstream neighboring boreholes. However, in the absence of such neighboring boreholes, $C(t)$ and $\overline{C}(t)$ become real numbers, aligning the imposed temperature gradient perfectly with the flow direction of the aquifer.

The remaining terms in Eq. (4) are imposed by the inner region onto the outer region and are intrinsic to the inner region's solution. In addition to the heat injection rate per unit borehole length $q(t)$, these terms involve the first harmonics $A_{0(+1)}(t)$ and $A_{0(-1)}(t)$ of the Fourier series expansion of the grout/ground temperature around the borehole wall. These harmonics correspond to the solution to the inner region without any convection, i.e., with zero Peclet number:

$$A_{0(\pm1)}(t) = \frac{1}{2\pi}\int_{-\pi}^{\pi} T\Big|_{r_0=r_b,\mathrm{Pe}=0} \mathrm{e}^{\mp\imath\theta_0}\,\mathrm{d}\theta_0.$$

The significance and rationale for this will become clear in Section 2.5, with further details and insights available in previous work by the authors [27,61].

2.4.2. Non-dimensionalization

The formulated heat transfer problem in the grout and ground is non-dimensionalized for convenience. For it, the borehole radius r_b is used to define the non-dimensional radial coordinates $\rho_0 = r_0/r_b$ and $\rho_j = r_j/r_b$, while $r_b^2/\alpha_g \sim t_b$ is used to define the non-dimensional time $\tau = \alpha_g t/r_b^2$.

The radial and azimuthal components of the velocity field are non-dimensionalized using the effective seepage velocity of the groundwater flow U_∞, so that

$$\mathrm{v}_\rho = \left(1 - \frac{1}{\rho_0^2}\right)\cos(\theta_0)$$

$$\mathrm{v}_\theta = -\left(1 + \frac{1}{\rho_0^2}\right)\sin(\theta_0).$$

Next, all heat injection rates are non-dimensionalized using a characteristic value q_c, which could be, for example, the mean or maximum value attained by $q_j(t)$ or $q(t)$:

$$\mathrm{q}_j = \frac{q_j}{q_c} \qquad \text{and} \qquad \mathrm{q} = \frac{q}{q_c}.$$

Finally, temperatures are non-dimensionalized with the characteristic temperature difference q_c/k_g so that

$$\Theta = \frac{T - T_\infty}{q_c/k_g} \qquad \text{and} \qquad \Theta_j = \frac{T_j - T_\infty}{q_c/k_g}.$$

With the introduced definitions for the non-dimensional variables, the energy conservation equations in grout and ground become, respectively,

$$0 = \frac{1}{\rho_0}\frac{\partial}{\partial\rho_0}\left(\rho_0\frac{\partial\Theta}{\partial\rho_0}\right) + \frac{1}{\rho_0^2}\frac{\partial^2\Theta}{\partial\theta_0^2}$$

and

$$\mathrm{Pe}\left[\mathrm{v}_\rho\frac{\partial\Theta}{\partial\rho_0} + \frac{\mathrm{v}_\theta}{\rho_0}\frac{\partial\Theta}{\partial\theta_0}\right] = \frac{1}{\rho_0}\frac{\partial}{\partial\rho_0}\left(\rho_0\frac{\partial\Theta}{\partial\rho_0}\right) + \frac{1}{\rho_0^2}\frac{\partial^2\Theta}{\partial\theta_0^2}, \tag{5}$$

while the non-dimensional continuity conditions at the borehole wall introduce the parameter $\kappa = k_b/k_g$:

$$\Theta\Big|_{\rho_0=1^-} = \Theta\Big|_{\rho_0=1^+}, \qquad -\kappa\frac{\partial\Theta}{\partial\rho_0}\Big|_{\rho_0=1^-} = -\frac{\partial\Theta}{\partial\rho_0}\Big|_{\rho_0=1^+}.$$

The heat injection rate per unit pipe length specified at pipe j non-dimensionalizes as follows:

$$\mathrm{q}_j(\tau) = \int_{-\pi}^{\pi} -\kappa\frac{\partial\Theta}{\partial\rho_j}\Big|_{\rho_j=\rho_{pj}} \rho_{pj}\,\mathrm{d}\theta_j,$$

with the non-dimensional pipe radius being $\rho_{pj} = r_{pj}/r_b$. The boundary condition specified then at the outer surface of pipe j introduces the non-dimensional pipe's inner thermal resistance $\mathrm{R}_{pj} = k_g R_{pj}$,

$$-\rho_{pj}\kappa\frac{\partial\Theta}{\partial\rho_j}\Big|_{\rho_j=\rho_{pj}} = \frac{\Theta_j(\tau) - \Theta\big|_{\rho_j=\rho_{pj}}}{\mathrm{R}_{pj}}.$$

The same non-dimensional quantity R_{pj} also appears in the expression that relates the non-dimensional fluid temperature in pipe j to the specified heat injection rate per unit pipe length:

$$\Theta_j(\tau) = \frac{\mathrm{R}_{pj}}{2\pi}\,\mathrm{q}_j(\tau) + \frac{1}{2\pi}\int_{-\pi}^{\pi}\Theta\Big|_{\rho_j=\rho_{pj}}\mathrm{d}\theta_j.$$

Finally, the matching condition enforced far from the borehole involves the non-dimensional counterparts of the temperature level and gradient imposed by the outer region,

$$\mathrm{A} = \frac{A - T_\infty}{q_c/k_g}, \qquad \mathrm{B} = \frac{B}{q_c/k_g}, \qquad \mathrm{C} = \frac{C}{q_c/k_g},$$

as well as the non-dimensional counterparts of the heat injection rate per unit borehole length and the first harmonics of the Fourier series expansion of the grout/ground temperature around the borehole wall:

$$\mathrm{q} = \sum_{j=1}^{N_p}\mathrm{q}_j \qquad \text{and} \qquad \mathrm{A}_{0(\pm1)} = \frac{A_{0(\pm1)}}{q_c/k_g}.$$

With all this, the matching condition non-dimensionalizes as

$$\begin{aligned}\rho_0 \to \infty:\ \Theta \to{}& \mathrm{A}(\tau) + \frac{\mathrm{q}(\tau)}{2\pi}\ln(\rho_0)\\ &+ \mathrm{Pe}\left[\mathrm{B}(\tau) + \mathrm{C}(\tau)\rho_0 \mathrm{e}^{+\imath\theta_0} + \overline{\mathrm{C}}(\tau)\rho_0\mathrm{e}^{-\imath\theta_0}\right]\\ &+ \mathrm{Pe}\left[\frac{\mathrm{A}_{0(+1)}(\tau) + \mathrm{A}_{0(-1)}(\tau)}{2} - \frac{\mathrm{q}(\tau)}{4\pi}\rho_0\cos(\theta_0)\right]\ln(\rho_0).\end{aligned}$$

2.5. Asymptotic expansion of inner problem

No exact solution is known for the formulated heat transfer problem. Consequently, an approximate solution is sought by exploiting the presence of a small parameter using asymptotic expansion techniques [38]. These methods expand the unknowns of the problem in powers of this small parameter, which, in the present case, is the Peclet number of the creeping groundwater flow. The resulting expansions for the grout/ground temperature and the fluid temperatures in the pipes are as follows:

$$\Theta = \Theta^{(0)} + \mathrm{Pe}\,\Theta^{(1)} + \mathcal{O}(\mathrm{Pe}^2)$$
$$\Theta_j = \Theta_j^{(0)} + \mathrm{Pe}\,\Theta_j^{(1)} + \mathcal{O}(\mathrm{Pe}^2).$$

It is well known that for two-dimensional convection–diffusion problems these expansions are not enough and so-called logarithmic switchback terms, which are powers of $1/\ln(\mathrm{Pe})$, need to be incorporated for completeness [38,62]. In this study, an unconventional approach is taken, treating these logarithmic terms as numerical constants inherent to the problem, thereby excluding them from the aforementioned expansions [27]. This approach significantly streamlines the analysis and resolution process without negatively affecting the obtained results.

The above expansions for the grout/ground temperature and the fluid temperatures in the pipes are then substituted into the formulated problem. Terms with equal powers of the Peclet number are grouped together to define a series of simpler problems whose sequential solution delivers the sought results. The following subsections detail the simplified problems corresponding to the first two terms of the expansions [27].

2.5.1. Zeroth-order problem

The zeroth-order solution, $\Theta^{(0)}$ and $\Theta_j^{(0)}$, is derived by solving the heat transfer problem that results from neglecting all terms of order Peclet and higher. This preserves the energy conservation equation in the grout, expressed as

$$0 = \frac{1}{\rho_0}\frac{\partial}{\partial\rho_0}\left(\rho_0\frac{\partial\Theta^{(0)}}{\partial\rho_0}\right) + \frac{1}{\rho_0^2}\frac{\partial^2\Theta^{(0)}}{\partial\theta_0^2},$$

while simplifying the energy conservation equation in the ground, Eq. (5), as the convective terms are of order Peclet. Consequently, the same differential equation governs the temperature distribution in both the grout and ground in the zeroth-order approximation of the problem.

The zeroth-order grout/ground temperature must also satisfy the continuity conditions at the borehole wall,

$$\Theta^{(0)}\Big|_{\rho_0=1^-} = \Theta^{(0)}\Big|_{\rho_0=1^+}, \qquad -\kappa\frac{\partial\Theta^{(0)}}{\partial\rho_0}\bigg|_{\rho_0=1^-} = -\frac{\partial\Theta^{(0)}}{\partial\rho_0}\bigg|_{\rho_0=1^+},$$

as well as the heat injection rates per unit pipe length $\mathrm{q}_j(\tau)$ specified at the N_p pipes inside the borehole:

$$\mathrm{q}_j(\tau) = \int_{-\pi}^{\pi} -\kappa\frac{\partial\Theta^{(0)}}{\partial\rho_j}\bigg|_{\rho_j=\rho_{pj}}\rho_{pj}\,\mathrm{d}\theta_j. \tag{6}$$

Also the additional boundary condition enforced at the outer surface of each pipe j must be obeyed by the zeroth-order grout/ground temperature,

$$-\rho_{pj}\kappa\frac{\partial\Theta^{(0)}}{\partial\rho_j}\bigg|_{\rho_j=\rho_{pj}} = \frac{\Theta_j^{(0)}(\tau) - \Theta^{(0)}\big|_{\rho_j=\rho_{pj}}}{\mathrm{R}_{pj}},$$

with the zeroth-order fluid temperature given by

$$\Theta_j^{(0)}(\tau) = \frac{\mathrm{R}_{pj}}{2\pi}\,\mathrm{q}_j(\tau) + \frac{1}{2\pi}\int_{-\pi}^{\pi}\Theta^{(0)}\Big|_{\rho_j=\rho_{pj}}\mathrm{d}\theta_j.$$

Finally the matching condition to enforce at the outer edge of the inner region is

$$\rho_0 \to \infty:\ \Theta^{(0)} \to \mathrm{A}(\tau) - \frac{\mathrm{q}(\tau)}{2\pi}\ln(\rho_0).$$

Once the zeroth-order grout/ground temperature is determined, the first harmonics $\mathrm{A}_{0(\pm1)}(\tau)$ of its Fourier series expansion around the borehole wall are computed. These harmonics are necessary for the matching condition in the subsequently formulated first-order problem:

$$\mathrm{A}_{0(\pm1)}(\tau) = \frac{1}{2\pi}\int_{-\pi}^{\pi}\Theta^{(0)}\Big|_{\rho_0=1}\mathrm{e}^{\mp\imath\theta_0}\,\mathrm{d}\theta_0.$$

2.5.2. First-order problem

The next level of approximation in the asymptotic expansion of the problem is achieved by retaining the terms of order Peclet. The energy conservation equation in the grout remains thereby unchanged:

$$0 = \frac{1}{\rho_0}\frac{\partial}{\partial\rho_0}\left(\rho_0\frac{\partial\Theta^{(1)}}{\partial\rho_0}\right) + \frac{1}{\rho_0^2}\frac{\partial^2\Theta^{(1)}}{\partial\theta_0^2}.$$

In contrast, the energy conservation equation in the ground now includes convective terms on its left-hand side. However, these are evaluated using the zeroth-order grout/ground temperature, causing the convective terms to act as forcing terms in the governing equation for $\Theta^{(1)}$:

$$\mathrm{v}_\rho\frac{\partial\Theta^{(0)}}{\partial\rho_0} + \frac{\mathrm{v}_\theta}{\rho_0}\frac{\partial\Theta^{(0)}}{\partial\theta_0} = \frac{1}{\rho_0}\frac{\partial}{\partial\rho_0}\left(\rho_0\frac{\partial\Theta^{(1)}}{\partial\rho_0}\right) + \frac{1}{\rho_0^2}\frac{\partial^2\Theta^{(1)}}{\partial\theta_0^2}.$$

Also the first-order correction to the grout/ground temperature must comply with the continuity conditions at the borehole wall:

$$\Theta^{(1)}\Big|_{\rho_0=1^-} = \Theta^{(1)}\Big|_{\rho_0=1^+}, \qquad -\kappa\frac{\partial\Theta^{(1)}}{\partial\rho_0}\bigg|_{\rho_0=1^-} = -\frac{\partial\Theta^{(1)}}{\partial\rho_0}\bigg|_{\rho_0=1^+}.$$

Regarding the specified heat injection rates per unit pipe length, $\mathrm{q}_j(\tau)$, the first-order correction to the grout/ground temperature does not need to satisfy these rates, as this requirement is already fulfilled by the zeroth-order solution through Eq. (6). Consequently, zero heat injection rates per unit pipe length must now be specified at the pipes to ensure that the overall problem accurately satisfies the given values for $\mathrm{q}_j(\tau)$:

$$0 = \int_{-\pi}^{\pi} -\kappa\frac{\partial\Theta^{(1)}}{\partial\rho_j}\bigg|_{\rho_j=\rho_{pj}}\rho_{pj}\,\mathrm{d}\theta_j.$$

The additional boundary condition enforced at the outer surface of each pipe j also appears in the first-order problem,

$$-\rho_{pj}\kappa\frac{\partial\Theta^{(1)}}{\partial\rho_j}\bigg|_{\rho_j=\rho_{pj}} = \frac{\Theta_j^{(1)}(\tau)-\Theta^{(1)}\big|_{\rho_j=\rho_{pj}}}{\mathrm{R}_{pj}},$$

with the first-order correction to the fluid temperatures being

$$\Theta_j^{(1)}(\tau) = \frac{1}{2\pi}\int_{-\pi}^{\pi}\Theta^{(1)}\big|_{\rho_j=\rho_{pj}}\mathrm{d}\theta_j.$$

Finally, the matching condition enforced at the outer rim of the inner region is in this case

$$\rho_0\to\infty:\ \Theta^{(1)}\to \mathrm{B}(\tau)+\mathrm{C}(\tau)\rho_0\mathrm{e}^{+\imath\theta_0}+\overline{\mathrm{C}}(\tau)\rho_0\mathrm{e}^{-\imath\theta_0} + \left[\frac{\mathrm{A}_{0(+1)}(\tau)+\mathrm{A}_{0(-1)}(\tau)}{2}-\frac{\mathrm{q}(\tau)}{4\pi}\rho_0\cos(\theta_0)\right]\ln(\rho_0).$$

To address the formulated first-order problem, its solution is divided into two parts by exploiting the linearity of the governing equations and boundary conditions. Thus, the first-order corrections to the grout/ground temperature and the fluid temperatures in the pipes are expressed as

$$\Theta^{(1)}=\Theta_{\mathrm{ex}}^{(1)}+\Theta_{\mathrm{en}}^{(1)} \qquad \text{and} \qquad \Theta_j^{(1)}=\Theta_{j,\mathrm{ex}}^{(1)}+\Theta_{j,\mathrm{en}}^{(1)}.$$

The exogenous first-order problem, comprising $\Theta_{\mathrm{ex}}^{(1)}$ and $\Theta_{j,\mathrm{ex}}^{(1)}$, accounts for the influence of the outer region on the inner region. This includes the temperature level $\mathrm{B}(\tau)$ and the temperature gradient specified by $\mathrm{C}(\tau)$ and $\overline{\mathrm{C}}(\tau)$. The governing equations and boundary conditions for this problem are summarized in Table 1.

The endogenous first-order problem, comprising $\Theta_{\mathrm{en}}^{(1)}$ and $\Theta_{j,\mathrm{en}}^{(1)}$, addresses aspects solely related to the inner region. This includes the forcing term in the energy conservation equation in the ground and all terms that the inner region imposes on the outer region through the matching condition. The governing equations and boundary conditions for this problem are summarized in Table 2.

Table 1
Formulation of exogenous first-order problem.

Energy conservation in ground:
$0=\frac{1}{\rho_0}\frac{\partial}{\partial\rho_0}\left(\rho_0\frac{\partial\Theta_{\mathrm{ex}}^{(1)}}{\partial\rho_0}\right)+\frac{1}{\rho_0^2}\frac{\partial^2\Theta_{\mathrm{ex}}^{(1)}}{\partial\theta_0^2}$
Energy conservation in grout:
$0=\frac{1}{\rho_0}\frac{\partial}{\partial\rho_0}\left(\rho_0\frac{\partial\Theta_{\mathrm{ex}}^{(1)}}{\partial\rho_0}\right)+\frac{1}{\rho_0^2}\frac{\partial^2\Theta_{\mathrm{ex}}^{(1)}}{\partial\theta_0^2}$
Continuity conditions at borehole wall:
$\Theta_{\mathrm{ex}}^{(1)}\big\vert_{\rho_0=1^-}=\Theta_{\mathrm{ex}}^{(1)}\big\vert_{\rho_0=1^+}$ and $-\kappa\frac{\partial\Theta_{\mathrm{ex}}^{(1)}}{\partial\rho_0}\big\vert_{\rho_0=1^-}=-\frac{\partial\Theta_{\mathrm{ex}}^{(1)}}{\partial\rho_0}\big\vert_{\rho_0=1^+}$
Boundary condition at wall of pipe j:
$-\rho_{pj}\kappa\frac{\partial\Theta_{\mathrm{ex}}^{(1)}}{\partial\rho_j}\big\vert_{\rho_j=\rho_{pj}}=\frac{\Theta_{j,\mathrm{ex}}^{(1)}(\tau)-\Theta_{\mathrm{ex}}^{(1)}\big\vert_{\rho_j=\rho_{pj}}}{\mathrm{R}_{pj}}$
with
$\Theta_{j,\mathrm{ex}}^{(1)}(\tau)=\frac{1}{2\pi}\int_{-\pi}^{\pi}\Theta_{\mathrm{ex}}^{(1)}\big\vert_{\rho_j=\rho_{pj}}\mathrm{d}\theta_j$
Matching condition far from borehole:
$\rho_0\to\infty:\ \Theta_{\mathrm{ex}}^{(1)}\to\mathrm{B}(\tau)+\mathrm{C}(\tau)\rho_0\mathrm{e}^{+\imath\theta_0}+\overline{\mathrm{C}}(\tau)\rho_0\mathrm{e}^{-\imath\theta_0}$

Table 2
Formulation of endogenous first-order problem.

Energy conservation in ground:
$\mathrm{v}_\rho\frac{\partial\Theta^{(0)}}{\partial\rho_0}+\frac{\mathrm{v}_\theta}{\rho_0}\frac{\partial\Theta^{(0)}}{\partial\theta_0}=\frac{1}{\rho_0}\frac{\partial}{\partial\rho_0}\left(\rho_0\frac{\partial\Theta_{\mathrm{en}}^{(1)}}{\partial\rho_0}\right)+\frac{1}{\rho_0^2}\frac{\partial^2\Theta_{\mathrm{en}}^{(1)}}{\partial\theta_0^2}$
with
$\mathrm{v}_\rho=\left(1-\frac{1}{\rho_0^2}\right)\cos(\theta_0)$ and $\mathrm{v}_\theta=-\left(1+\frac{1}{\rho_0^2}\right)\sin(\theta_0)$
Energy conservation in grout:
$0=\frac{1}{\rho_0}\frac{\partial}{\partial\rho_0}\left(\rho_0\frac{\partial\Theta_{\mathrm{en}}^{(1)}}{\partial\rho_0}\right)+\frac{1}{\rho_0^2}\frac{\partial^2\Theta_{\mathrm{en}}^{(1)}}{\partial\theta_0^2}$
Continuity conditions at borehole wall:
$\Theta_{\mathrm{en}}^{(1)}\big\vert_{\rho_0=1^-}=\Theta_{\mathrm{en}}^{(1)}\big\vert_{\rho_0=1^+}$ and $-\kappa\frac{\partial\Theta_{\mathrm{en}}^{(1)}}{\partial\rho_0}\big\vert_{\rho_0=1^-}=-\frac{\partial\Theta_{\mathrm{en}}^{(1)}}{\partial\rho_0}\big\vert_{\rho_0=1^+}$
Boundary condition at wall of pipe j:
$-\rho_{pj}\kappa\frac{\partial\Theta_{\mathrm{en}}^{(1)}}{\partial\rho_j}\big\vert_{\rho_j=\rho_{pj}}=\frac{\Theta_{j,\mathrm{en}}^{(1)}(\tau)-\Theta_{\mathrm{en}}^{(1)}\big\vert_{\rho_j=\rho_{pj}}}{\mathrm{R}_{pj}}$
with
$\Theta_{j,\mathrm{en}}^{(1)}(\tau)=\frac{1}{2\pi}\int_{-\pi}^{\pi}\Theta_{\mathrm{en}}^{(1)}\big\vert_{\rho_j=\rho_{pj}}\mathrm{d}\theta_j$
Matching condition far from borehole:
$\rho_0\to\infty:\ \Theta_{\mathrm{en}}^{(1)}\to\left[\frac{\mathrm{A}_{0(+1)}(\tau)+\mathrm{A}_{0(-1)}(\tau)}{2}-\frac{\mathrm{q}(\tau)}{4\pi}\rho_0\cos(\theta_0)\right]\ln(\rho_0)$
with
$\mathrm{A}_{0(\pm1)}(\tau)=\frac{1}{2\pi}\int_{-\pi}^{\pi}\Theta^{(0)}\big\vert_{\rho_0=1}\mathrm{e}^{\mp\imath\theta_0}\,\mathrm{d}\theta_0$

3. Modified enhanced multipole method

To solve the three problems formulated in the previous section, the enhanced multipole method is employed [40,41]. This method provides the exact solution to the quasi-steady heat conduction problem in grout and ground, thus yielding the exact solution to the zeroth-order problem formulated in Section 2.5.1.

For the exogenous and endogenous first-order problems, summarized in Tables 1 and 2, the enhanced multipole method must be modified to account for the presence of forcing terms in the governing equation in the ground and a temperature gradient in the matching condition. The resulting procedure, termed the modified enhanced multipole method, is described in the present section.

3.1. Multipole expansion

The enhanced multipole method involves expanding the grout and ground temperature using conveniently chosen functions F_{in}, commonly referred to as multipoles in the literature [13,14,40,41,63]. Each pipe i contributes an infinite number of these functions, with subindex n indicating the azimuthal order of each multipole. The expansion of the grout/ground temperature is then expressed as follows:

$$\Theta(\rho_0,\theta_0,\tau)=\Theta_p(\rho_0,\theta_0,\tau)+\sum_{i=1}^{N_p}\sum_{n=-\infty}^{\infty}C_{in}(\tau)F_{in}(\rho_0,\theta_0). \tag{7}$$

Each multipole F_{in} is obtained from solving a quasi-steady heat conduction problem in grout and ground [41],

$$0=\frac{1}{\rho_0}\frac{\partial}{\partial\rho_0}\left(\rho_0\frac{\partial F_{in}}{\partial\rho_0}\right)+\frac{1}{\rho_0^2}\frac{\partial^2F_{in}}{\partial\theta_0^2},$$

with its continuity conditions at the borehole wall:

$$F_{in}\big|_{\rho_0=1^-}=F_{in}\big|_{\rho_0=1^+}, \qquad -\kappa\frac{\partial F_{in}}{\partial\rho_0}\bigg|_{\rho_0=1^-}=-\frac{\partial F_{in}}{\partial\rho_0}\bigg|_{\rho_0=1^+}.$$

Different behaviors far from the borehole are enforced depending on n. While for $n\neq0$ the corresponding multipole F_{in} decays to zero,

$$\rho_0\to\infty:\ F_{in}\to0,$$

for $n=0$ the multipole F_{i0} grows logarithmically as

$$\rho_0\to\infty:\ F_{i0}\to-\kappa\ln(\rho_0).$$

Finally, each multipole F_{in} is allowed to diverge at the center of its pipe i.

Explicit expressions for the multipoles F_{in} are provided in the literature in terms of the eigenfunctions of the underlying mathematical

problem [40]. However, these expressions are not necessary for the theoretical considerations of this work or for the numerical examples presented in Section 7.

The proposed expansion for the grout/ground temperature also includes a particular solution to the problem, denoted as Θ_p. This particular solution incorporates all aspects not covered by the multipoles F_{in}, such as the forcing terms in the governing equation in the ground and the influences exerted by the outer region on the inner region.

Finally, the proposed expansion includes a-priori unknown weights C_{in} which multiply the corresponding multipoles F_{in}. Their values are determined by ensuring the expansion of the grout/ground temperature satisfies the boundary conditions at the N_p pipes. That is, the specified heat injection rates per unit pipe length,

$$\int_{-\pi}^{\pi} \rho_{pj} \frac{\partial \Theta}{\partial \rho_j}\bigg|_{\rho_j=\rho_{pj}} \mathrm{d}\theta_j = -\frac{\mathrm{q}_j(\tau)}{\kappa}, \tag{8}$$

and the additional boundary condition enforced at the outer surface of the pipes:

$$-\kappa \mathrm{R}_{pj} \rho_{pj} \frac{\partial \Theta}{\partial \rho_j}\bigg|_{\rho_j=\rho_{pj}} = \Theta_j(\tau) - \Theta\big|_{\rho_j=\rho_{pj}}. \tag{9}$$

3.2. Fourier expansion of F_{in} and Θ_p

To enforce the previous two conditions at the pipes, the Fourier series expansion of the grout/ground temperature around each pipe j is obtained. For this purpose, the Fourier series expansions of the multipole F_{in} and its derivative with respect to ρ_j are employed [41]:

$$F_{in}\big|_{\rho_j=\rho_{pj}} = \sum_{m=-\infty}^{\infty} \mathcal{F}_{injm}\, \mathrm{e}^{\imath m\theta_j}$$

$$\rho_{pj} \frac{\partial F_{in}}{\partial \rho_j}\bigg|_{\rho_j=\rho_{pj}} = \sum_{m=-\infty}^{\infty} \mathcal{F}'_{injm}\, \mathrm{e}^{\imath m\theta_j},$$

with the Fourier series coefficients being

$$\mathcal{F}_{injm} = \frac{1}{2\pi}\int_{-\pi}^{\pi} F_{in}\, \mathrm{e}^{-\imath m\theta_j}\, \mathrm{d}\theta_j\bigg|_{\rho_j=\rho_{pj}}$$

$$\mathcal{F}'_{injm} = \rho_{pj} \frac{\partial \mathcal{F}_{injm}}{\partial \rho_{pj}}.$$

Explicit expressions for $\mathcal{F}_{injm}$ and $\mathcal{F}'_{injm}$ are readily available in the literature [40]. These expressions are necessary for certain theoretical considerations in this work as well as for the numerical examples presented in Section 7.

The Fourier series expansions of the particular solution Θ_p and its derivative with respect to ρ_j are defined following the same approach as for the multipoles:

$$\Theta_p\big|_{\rho_j=\rho_{pj}} = \sum_{m=-\infty}^{\infty} \mathcal{P}_{jm}\, \mathrm{e}^{\imath m\theta_j}$$

$$\rho_{pj} \frac{\partial \Theta_p}{\partial \rho_j}\bigg|_{\rho_j=\rho_{pj}} = \sum_{m=-\infty}^{\infty} \mathcal{P}'_{jm}\, \mathrm{e}^{\imath m\theta_j},$$

with the Fourier series coefficients being given by

$$\mathcal{P}_{jm} = \frac{1}{2\pi}\int_{-\pi}^{\pi} \Theta_p\, \mathrm{e}^{-\imath m\theta_j}\, \mathrm{d}\theta_j\bigg|_{\rho_j=\rho_{pj}},$$

$$\mathcal{P}'_{jm} = \rho_{pj} \frac{\partial \mathcal{P}_{jm}}{\partial \rho_{pj}}.$$

As the particular solution Θ_p varies with time, its coefficients $\mathcal{P}_{jm}$ and $\mathcal{P}'_{jm}$ also turn into functions of τ. This differs from the Fourier series coefficients $\mathcal{F}_{injm}$ and $\mathcal{F}'_{injm}$, which, under the assumption of slowly-varying heat injection rates, remain independent of time [40]. For simplicity, the time dependence of $\mathcal{P}_{jm}$ and $\mathcal{P}'_{jm}$, as well as of C_{in}, q_j, and A_{0m}, will be explicitly indicated only where necessary or convenient.

3.3. Heat injection rates enforcement

To enforce the prescribed heat injection rates per unit pipe length $\mathrm{q}_j(\tau)$, the multipole expansion for the grout/ground temperature, as given in Eq. (7), is inserted into Eq. (8):

$$\int_{-\pi}^{\pi} \left[\rho_{pj} \frac{\partial \Theta_p}{\partial \rho_j}\bigg|_{\rho_j=\rho_{pj}} + \sum_{i=1}^{N_p} \sum_{n=-\infty}^{\infty} C_{in} \rho_{pj} \frac{\partial F_{in}}{\partial \rho_j}\bigg|_{\rho_j=\rho_{pj}} \right] \mathrm{d}\theta_j = -\frac{\mathrm{q}_j}{\kappa}.$$

Substituting the Fourier series expansions of F_{in} and Θ_p for their radial derivatives around pipe j yields

$$\int_{-\pi}^{\pi} \sum_{m=-\infty}^{\infty} \left[\mathcal{P}'_{jm} + \sum_{i=1}^{N_p} \sum_{n=-\infty}^{\infty} C_{in} \mathcal{F}'_{injm} \right] \mathrm{e}^{\imath m\theta_j}\, \mathrm{d}\theta_j = -\frac{\mathrm{q}_j}{\kappa}.$$

Azimuthal integration of all terms in the Fourier series expansion around pipe j reveals that the only non-zero contribution to the resulting expression comes from $m = 0$:

$$\sum_{i=1}^{N_p} \sum_{n=-\infty}^{\infty} C_{in} \mathcal{F}'_{inj0} = -\frac{\mathrm{q}_j}{2\pi\kappa} - \mathcal{P}'_{j0}. \tag{10}$$

In contrast to the original enhanced multipole method [40,41], a new term emerges on the right-hand side of the equation. This term represents the heat injection rate per unit pipe length at pipe j due to the particular solution Θ_p.

3.4. Boundary condition at pipe walls enforcement

Substituting the multipole expansion for the grout/ground temperature, Eq. (7), into the boundary condition enforced at the outer surface of the pipes, Eq. (9), yields

$$-\kappa \mathrm{R}_{pj} \left[\rho_{pj} \frac{\partial \Theta_p}{\partial \rho_j}\bigg|_{\rho_j=\rho_{pj}} + \sum_{i=1}^{N_p} \sum_{n=-\infty}^{\infty} C_{in} \rho_{pj} \frac{\partial F_{in}}{\partial \rho_j}\bigg|_{\rho_j=\rho_{pj}} \right] = \Theta_j - \left[\Theta_p\big|_{\rho_j=\rho_{pj}} + \sum_{i=1}^{N_p} \sum_{n=-\infty}^{\infty} C_{in} F_{in}\big|_{\rho_j=\rho_{pj}} \right].$$

Utilizing the Fourier series expansions around pipe j of Θ_p and F_{in}, as well as their derivatives with respect to ρ_j, allows the previous expression to be rewritten as

$$\sum_{m=-\infty}^{\infty} \sum_{i=1}^{N_p} \sum_{n=-\infty}^{\infty} C_{in} \left[\mathcal{F}_{injm} - \kappa \mathrm{R}_{pj} \mathcal{F}'_{injm} \right] \mathrm{e}^{\imath m\theta_j} = \Theta_j - \sum_{m=-\infty}^{\infty} \left[\mathcal{P}_{jm} - \kappa \mathrm{R}_{pj} \mathcal{P}'_{jm} \right] \mathrm{e}^{\imath m\theta_j}.$$

This condition can now be enforced independently for each harmonic of the Fourier series expansion around pipe j, resulting in an infinite set of linear algebraic equations, with m ranging from $-\infty$ to $+\infty$, where δ_{m0} represents Kronecker's delta:

$$\sum_{i=1}^{N_p} \sum_{n=-\infty}^{\infty} C_{in} \left[\mathcal{F}_{injm} - \kappa \mathrm{R}_{pj} \mathcal{F}'_{injm} \right] = \Theta_j \delta_{m0} - \left[\mathcal{P}_{jm} - \kappa \mathrm{R}_{pj} \mathcal{P}'_{jm} \right]. \tag{11}$$

In contrast to the original enhanced multipole method [40,41], these equations feature additional terms on their right-hand sides. While in the enhanced multipole method only the equations with m=0 present additional terms to Θ_j, all equal to the apparent ground temperature, now contributions from the particular solution Θ_p are present in all equations, no matter the value of m.

3.5. Fluid temperatures

An infinite system of linear algebraic equations is solved to determine the values of the weights C_{in} required for the expansion of the grout/ground temperature, Eq. (7), to meet the boundary conditions

at the N_p pipes. This system consists of Eq. (10) and all equations in Eq. (11) where $m \neq 0$. Thus,

$$\begin{aligned} \sum_{i=1}^{N_p} \sum_{n=-\infty}^{\infty} C_{in} \mathcal{F}'_{inj0} &= -\frac{\mathrm{q}_j}{2\pi\kappa} - \mathcal{P}'_{j0} \\ \sum_{i=1}^{N_p} \sum_{n=-\infty}^{\infty} C_{in} \left[\mathcal{F}_{injm} - \kappa \mathrm{R}_{pj} \mathcal{F}'_{injm} \right] &= -\left[\mathcal{P}_{jm} - \kappa \mathrm{R}_{pj} \mathcal{P}'_{jm} \right], \end{aligned} \tag{12}$$

where index j ranges from 1 to N_p in both sets of equations, and index m ranges from $-\infty$ to $+\infty$ excluding $m = 0$.

Once the weights C_{in} are determined, the N_p fluid temperatures Θ_j that ensure the prescribed heat injection rates per unit pipe length are met result from the N_p equations in Eq. (11) with $m = 0$:

$$\sum_{i=1}^{N_p} \sum_{n=-\infty}^{\infty} C_{in} \left[\mathcal{F}_{inj0} - \kappa \mathrm{R}_{pj} \mathcal{F}'_{inj0} \right] = \Theta_j - \left[\mathcal{P}_{j0} - \kappa \mathrm{R}_{pj} \mathcal{P}'_{j0} \right]. \tag{13}$$

3.6. Temperature around the borehole wall

Besides the fluid temperatures Θ_j, another valuable result for the present work is the temperature distribution around the borehole wall. Particularizing Eq. (7) at the borehole wall, where $\rho_0 = 1$, yields

$$\Theta\Big|_{\rho_0=1} = \Theta_p\Big|_{\rho_0=1} + \sum_{i=1}^{N_p} \sum_{n=-\infty}^{\infty} C_{in} F_{in}\Big|_{\rho_0=1}.$$

If the borehole is considered merely another pipe, denoted as pipe 0 with $\rho_{p0} = 1$ [40,41], this expression for the temperature distribution along the borehole wall can also be expressed as

$$\Theta\Big|_{\rho_0=1} = \sum_{m=-\infty}^{\infty} \left[\mathcal{P}_{0m} + \sum_{i=1}^{N_p} \sum_{n=-\infty}^{\infty} C_{in} \mathcal{F}_{in0m} \right] \mathrm{e}^{\imath m \theta_0}, \tag{14}$$

with Fourier series coefficients $\mathcal{P}_{0m}$ and $\mathcal{F}_{in0m}$ being fully equivalent to the ones defined in Section 3.2. Additionally, explicit expressions for $\mathcal{F}_{in0m}$ are readily available in the literature [40].

4. Solution to inner problem

The modified enhanced multipole method is employed next to address all three problems formulated in Section 2.5. By properly combining their solutions, Sections 5 and 6 will yield the desired conclusions regarding the impact of creeping groundwater flows on the network of thermal resistances and the apparent ground temperature.

4.1. Zeroth-order solution

The first problem to address is the zeroth-order one formulated in Section 2.5.1. Since there are no forcing terms in the governing equations, the only phenomenon to incorporate into the particular solution Θ_p is the temperature level $\mathrm{A}(\tau)$ imposed by the outer region onto the inner region. Consequently, $\Theta_p = \mathrm{A}(\tau)$.

Next, the coefficients $\mathcal{P}_{jm}$ and $\mathcal{P}'_{jm}$ of the Fourier series expansions around pipe j for Θ_p and its derivative with respect to ρ_j are obtained. Since the particular solution is uniform in space, they are straightforward to determine:

$$\mathcal{P}_{jm} = \mathrm{A}(\tau)\, \delta_{m0}, \qquad \mathcal{P}'_{jm} = 0. \tag{15}$$

These Fourier series coefficients are then substituted into Eq. (12) to derive the infinite system of linear algebraic equations whose solution yields the weights C_{in}:

$$\begin{aligned} \sum_{i=1}^{N_p} \sum_{n=-\infty}^{\infty} C_{in} \mathcal{F}'_{inj0} &= -\frac{\mathrm{q}_j}{2\pi\kappa} \\ \sum_{i=1}^{N_p} \sum_{n=-\infty}^{\infty} C_{in} \left[\mathcal{F}_{injm} - \kappa \mathrm{R}_{pj} \mathcal{F}'_{injm} \right] &= 0, \end{aligned}$$

where index j ranges from 1 to N_p in both sets of equations, and index m ranges from $-\infty$ to $+\infty$ excluding $m = 0$.

This system of equations coincides with the one solved by the original enhanced multipole method [40,41]. This is expected as the zeroth-order problem is a purely conductive one, with no additional imposition by the outer region other than a spatially uniform temperature level.

The original enhanced multipole method expresses the solution to the formulated system of equations as a linear combination of the heat injection rates per unit pipe length $\mathrm{q}_j(\tau)$ [40,41]. A similar approach is adopted here, expressing the weights C_{in} as follows:

$$C_{in}(\tau) = \sum_{a=1}^{N_p} C_{ina} \frac{\mathrm{q}_a(\tau)}{2\pi\kappa}. \tag{16}$$

Substituting this relationship into the formulated system of linear algebraic equations results in an alternative system of equations directly for the subweights C_{ina}. In this system, the indices j and a range from 1 to N_p in both sets of equations, and index m ranges from $-\infty$ to $+\infty$ excluding $m = 0$:

$$\begin{aligned} \sum_{i=1}^{N_p} \sum_{n=-\infty}^{\infty} C_{ina} \mathcal{F}'_{inj0} &= -\delta_{aj} \\ \sum_{i=1}^{N_p} \sum_{n=-\infty}^{\infty} C_{ina} \left[\mathcal{F}_{injm} - \kappa \mathrm{R}_{pj} \mathcal{F}'_{injm} \right] &= 0. \end{aligned} \tag{17}$$

Once the subweights C_{ina}, which are time-independent, are determined, the zeroth-order fluid temperatures $\Theta_j^{(0)}(\tau)$ can be obtained. This is done by combining Eq. (16) with Eq. (13) and the values for $\mathcal{P}_{j0}$ and $\mathcal{P}'_{j0}$:

$$\sum_{i=1}^{N_p} \sum_{n=-\infty}^{\infty} \sum_{a=1}^{N_p} C_{ina} \left[\mathcal{F}_{inj0} - \kappa \mathrm{R}_{pj} \mathcal{F}'_{inj0} \right] \frac{\mathrm{q}_a(\tau)}{2\pi\kappa} = \Theta_j^{(0)}(\tau) - \mathrm{A}(\tau).$$

4.1.1. Network of thermal resistances

The final result of the previous section can be conveniently reinterpreted as a network of thermal resistances, resulting in the mathematically equivalent expression

$$\sum_{j=1}^{N_p} \hat{\mathrm{R}}_{ij}^{(0)} \mathrm{q}_j(\tau) = \Theta_i^{(0)}(\tau) - \Theta_{ai}^{(0)}(\tau).$$

The zeroth-order thermal resistances $\hat{\mathrm{R}}_{ij}^{(0)}$, which do not depend on time, are given by

$$\begin{aligned} 2\pi\kappa \hat{\mathrm{R}}_{ij}^{(0)} &= \sum_{a=1}^{N_p} \sum_{n=-\infty}^{\infty} C_{anj} \left[\mathcal{F}_{ani0} - \kappa \mathrm{R}_{pi} \mathcal{F}'_{ani0} \right] \\ &= \kappa \mathrm{R}_{pi} \delta_{ij} + \sum_{a=1}^{N_p} \sum_{n=-\infty}^{\infty} C_{anj} \mathcal{F}_{ani0}, \end{aligned}$$

where the latter expression is derived by simplifying the former using the first set of equations in Eq. (17).

The zeroth-order apparent ground temperature for pipe i, $\Theta_{ai}^{(0)}(\tau)$, is equal to the temperature level $\mathrm{A}(\tau)$ imposed by the outer region onto the inner region. Consequently, in the zeroth-order approximation of the problem, all apparent ground temperatures for the pipes are equal:

$$\Theta_{ai}^{(0)}(\tau) = \mathrm{A}(\tau).$$

4.1.2. Borehole wall harmonics

The grout/ground temperature distribution around the borehole wall is determined next, as its Fourier series expansion is required for solving the endogenous first-order problem. The coefficients of this Fourier series expansion are given by

$$\mathrm{A}_{0m}(\tau) = \frac{1}{2\pi} \int_{-\pi}^{\pi} \Theta^{(0)}\Big|_{\rho_0=1} \mathrm{e}^{-\imath m \theta_0} \mathrm{d}\theta_0.$$

Using Eq. (14) for the temperature around the borehole wall, the Fourier series coefficients are directly obtained:

$$\mathrm{A}_{0m}(\tau) = \mathcal{P}_{0m}(\tau) + \sum_{i=1}^{N_p} \sum_{n=-\infty}^{\infty} C_{in}(\tau) \mathcal{F}_{in0m}.$$

Taking into account Eq. (15) for $\mathcal{P}_{0m}$ and the linear dependence of the weights C_{in} on the heat injection rates per unit pipe length $\mathrm{q}_j(\tau)$, Eq. (16), yields

$$\mathrm{A}_{0m}(\tau) = \mathrm{A}(\tau)\, \delta_{m0} + \sum_{a=1}^{N_p} \mathrm{A}_{0ma} \frac{\mathrm{q}_a(\tau)}{2\pi\kappa},$$

where the weights A_{0ma} do not depend on time and are given by

$$\mathrm{A}_{0ma} = \sum_{i=1}^{N_p} \sum_{n=-\infty}^{\infty} C_{ina} \mathcal{F}_{in0m}.$$

4.2. Exogenous first-order correction

The second problem to address is the exogenous first-order problem summarized in Table 1. In this case, the particular solution Θ_p includes both the imposed temperature level $\mathrm{B}(\tau)$ and the thermal response to the imposed temperature gradient specified by $\mathrm{C}(\tau)$ and $\overline{\mathrm{C}}(\tau)$.

To obtain the latter, the particular solution must satisfy the governing equations in both the grout and ground, as well as the continuity conditions at the borehole wall. This is achieved with the aid of the Appendix, leading to the following expressions for the particular solution:

$$\Theta_p = \begin{cases} \mathrm{B}(\tau) + \dfrac{2\rho_0}{1+\kappa} \left(\mathrm{C}(\tau)\, \mathrm{e}^{+\imath\theta_0} + \overline{\mathrm{C}}(\tau)\, \mathrm{e}^{-\imath\theta_0} \right) & \text{if } \rho_0 \le 1 \\ \mathrm{B}(\tau) + \left[\rho_0 + \dfrac{1-\kappa}{1+\kappa} \dfrac{1}{\rho_0} \right] \left(\mathrm{C}(\tau)\, \mathrm{e}^{+\imath\theta_0} + \overline{\mathrm{C}}(\tau)\, \mathrm{e}^{-\imath\theta_0} \right) & \text{if } \rho_0 \ge 1. \end{cases}$$

Next, the coefficients of the Fourier series expansions around pipe j for Θ_p and its derivative with respect to ρ_j are obtained. To calculate them, complex arithmetic is used to express the position (ρ_0, θ_0) in the polar coordinate system centered at the borehole in terms of the position (ρ_j, θ_j) in the polar coordinate system centered at pipe j:

$$\rho_0 \mathrm{e}^{\pm\imath\theta_0} = \rho_{0j} \mathrm{e}^{\pm\imath\theta_{0j}} + \rho_{pj} \mathrm{e}^{\pm\imath\theta_j}.$$

By combining this relationship with the expression for Θ_p valid inside the borehole, where $\rho_0 \le 1$, it can be shown that all Fourier series coefficients $\mathcal{P}_{jm}$ and $\mathcal{P}'_{jm}$ with $|m| > 1$ are zero. For $m = 0$, the coefficients are given by

$$\mathcal{P}_{j0}(\tau) = \mathrm{B}(\tau) + \frac{2\rho_{0j}}{1+\kappa} \left(\mathrm{C}(\tau)\, \mathrm{e}^{+\imath\theta_{0j}} + \overline{\mathrm{C}}(\tau)\, \mathrm{e}^{-\imath\theta_{0j}} \right)$$

and $\mathcal{P}'_{j0} = 0$, while for $m = \pm 1$ they are given by

$$\mathcal{P}_{j(+1)}(\tau) = \mathcal{P}'_{j(+1)}(\tau) = \frac{2\rho_{pj}}{1+\kappa} \mathrm{C}(\tau)$$

$$\mathcal{P}_{j(-1)}(\tau) = \mathcal{P}'_{j(-1)}(\tau) = \frac{2\rho_{pj}}{1+\kappa} \overline{\mathrm{C}}(\tau).$$

Thereafter, weights C_{in} are determined by substituting the previous Fourier series coefficients into Eq. (12). When writing the resulting system of linear algebraic equations, two additional remarks need to be made. First, in the exogenous first-order problem, no heat injection rates per unit pipe length are specified at the pipes, so the first set of equations in Eq. (12) will have zero right-hand sides. Second, only $\mathrm{C}(\tau)$ and $\overline{\mathrm{C}}(\tau)$ trigger the thermal response of the inner region. Consequently, weights C_{in} can be expressed as linear combinations of these two quantities:

$$C_{in}(\tau) = C_{in,\mathrm{c}} \mathrm{C}(\tau) + C_{in,\bar{\mathrm{c}}} \overline{\mathrm{C}}(\tau).$$

Substituting this relationship into Eq. (12) yields independent systems of linear algebraic equations for each set of subweights $C_{in,\mathrm{c}}$ and $C_{in,\bar{\mathrm{c}}}$. Thus, the equations to solve for the former set are

$$\begin{aligned} &\sum_{i=1}^{N_p} \sum_{n=-\infty}^{\infty} C_{in,\mathrm{c}} \mathcal{F}'_{inj0} = 0 \\ &\sum_{i=1}^{N_p} \sum_{n=-\infty}^{\infty} C_{in,\mathrm{c}} \left[\mathcal{F}_{injm} - \kappa \mathrm{R}_{pj} \mathcal{F}'_{injm} \right] = 0 \qquad \forall m \ne 0, +1 \\ &\sum_{i=1}^{N_p} \sum_{n=-\infty}^{\infty} C_{in,\mathrm{c}} \left[\mathcal{F}_{inj(+1)} - \kappa \mathrm{R}_{pj} \mathcal{F}'_{inj(+1)} \right] = -\left[1 - \kappa \mathrm{R}_{pj} \right] \frac{2\rho_{pj}}{1+\kappa}, \end{aligned} \tag{18}$$

while the equations to solve for the latter set are

$$\begin{aligned} &\sum_{i=1}^{N_p} \sum_{n=-\infty}^{\infty} C_{in,\bar{\mathrm{c}}} \mathcal{F}'_{inj0} = 0 \\ &\sum_{i=1}^{N_p} \sum_{n=-\infty}^{\infty} C_{in,\bar{\mathrm{c}}} \left[\mathcal{F}_{injm} - \kappa \mathrm{R}_{pj} \mathcal{F}'_{injm} \right] = 0 \qquad \forall m \ne 0, -1 \\ &\sum_{i=1}^{N_p} \sum_{n=-\infty}^{\infty} C_{in,\bar{\mathrm{c}}} \left[\mathcal{F}_{inj(-1)} - \kappa \mathrm{R}_{pj} \mathcal{F}'_{inj(-1)} \right] = -\left[1 - \kappa \mathrm{R}_{pj} \right] \frac{2\rho_{pj}}{1+\kappa}. \end{aligned} \tag{19}$$

In both cases, the index j ranges from 1 to N_p, and the middle set of equations applies to all values of m ranging from $-\infty$ to $+\infty$, excluding the two values specified on the right.

Once the subweights $C_{in,\mathrm{c}}$ and $C_{in,\bar{\mathrm{c}}}$ are known, obtained by solving the previous two systems of linear algebraic equations, the exogenous first-order corrections $\Theta^{(1)}_{j,\mathrm{ex}}(\tau)$ for the fluid temperatures in the pipes are determined by Eq. (13):

$$\sum_{i=1}^{N_p} \sum_{n=-\infty}^{\infty} \left[C_{in,\mathrm{c}} \mathrm{C}(\tau) + C_{in,\bar{\mathrm{c}}} \overline{\mathrm{C}}(\tau) \right] \left[\mathcal{F}_{inj0} - \kappa \mathrm{R}_{pj} \mathcal{F}'_{inj0} \right] = \Theta^{(1)}_{j,\mathrm{ex}}(\tau) - \mathcal{P}_{j0}(\tau).$$

The term $\mathcal{P}_{j0}(\tau)$ has not been substituted for the sake of clarity and compactness.

4.2.1. Network of thermal resistances

The last expression can be conveniently reinterpreted as a network of thermal resistances, leading to the mathematically equivalent expression

$$0 = \Theta^{(1)}_{i,\mathrm{ex}}(\tau) - \Theta^{(1)}_{ai}(\tau).$$

Since the prescribed heat injection rates per unit pipe length $\mathrm{q}_j(\tau)$ do not participate in the exogenous first-order problem, no left-hand side appears in the expression.

The first-order correction to the apparent ground temperature for pipe i is defined as

$$\Theta^{(1)}_{ai}(\tau) = \mathcal{P}_{i0}(\tau) + \sum_{a=1}^{N_p} \sum_{n=-\infty}^{\infty} \left[C_{an,\mathrm{c}} \mathrm{C}(\tau) + C_{an,\bar{\mathrm{c}}} \overline{\mathrm{C}}(\tau) \right] \mathcal{F}_{ani0},$$

where advantage has been taken of the first set of equations in Eqs. (18) and (19). Substituting $\mathcal{P}_{i0}(\tau)$ and rearranging the output leads to

$$\begin{aligned} \Theta^{(1)}_{ai}(\tau) = \mathrm{B}(\tau) &+ \left[\frac{2\rho_{0i}}{1+\kappa} \mathrm{e}^{+\imath\theta_{0i}} + \sum_{a=1}^{N_p} \sum_{n=-\infty}^{\infty} C_{an,\mathrm{c}} \mathcal{F}_{ani0} \right] \mathrm{C}(\tau) \\ &+ \left[\frac{2\rho_{0i}}{1+\kappa} \mathrm{e}^{-\imath\theta_{0i}} + \sum_{a=1}^{N_p} \sum_{n=-\infty}^{\infty} C_{an,\bar{\mathrm{c}}} \mathcal{F}_{ani0} \right] \overline{\mathrm{C}}(\tau). \end{aligned}$$

The first term, $B(\tau)$, is common to all pipes and represents a correction to the uniform temperature level $A(\tau)$ defining the zeroth-order apparent ground temperatures for the pipes. The remaining terms are due to the temperature gradient imposed by the outer region on the inner region. The first part of the coefficients multiplying $C(\tau)$ and $\overline{C}(\tau)$ is the particular solution evaluated at the position of pipe i, while the second part is the thermal response of the inner region to that particular solution.

The dependence of the apparent ground temperatures for the pipes on the thermal response of the inner region complicates their computation compared to purely conductive grounds, as both regions are now interwoven and can no longer be treated separately.

4.3. Endogenous first-order correction

The final problem to address is the endogenous first-order problem summarized in Table 2. The particular solution Θ_p now includes all forcing terms present in the governing equation for the ground and all terms imposed by the inner region on the outer region. This makes Θ_p significantly more complex, so its derivation is detailed in the Appendix. The same applies to the corresponding Fourier series coefficients $\mathcal{P}_{jm}(\tau)$ and $\mathcal{P}'_{jm}(\tau)$.

Next, the weights $C_{in}(\tau)$ are determined by substituting the Fourier series coefficients given in the Appendix into Eq. (12). Significantly, $\mathcal{P}'_{j0}(\tau) = 0$, which combined with the absence of specified heat injection rates per unit pipe length, leads to zero right-hand sides in the first set of equations in Eq. (12).

Additionally, the Appendix shows that $\mathcal{P}_{jm}(\tau)$ and $\mathcal{P}'_{jm}(\tau)$ are linear combinations of the heat injection rates per unit pipe length specified at the pipes. This dependency arises from the presence of the zeroth-order solution in the forcing terms of the governing equation in the ground. Thus, the Fourier series coefficients $\mathcal{P}_{jm}(\tau)$ and $\mathcal{P}'_{jm}(\tau)$ can be expressed as

$$\mathcal{P}_{jm}(\tau) = \sum_{a=1}^{N_p} \mathcal{P}_{jma} \frac{\mathrm{q}_a(\tau)}{2\pi\kappa} \quad \text{and} \quad \mathcal{P}'_{jm}(\tau) = \sum_{a=1}^{N_p} \mathcal{P}'_{jma} \frac{\mathrm{q}_a(\tau)}{2\pi\kappa},$$

which implies that the weights $C_{in}(\tau)$ can also be expressed as linear combinations of the heat injection rates per unit pipe length specified at the pipes:

$$C_{in}(\tau) = \sum_{a=1}^{N_p} C_{ina} \frac{\mathrm{q}_a(\tau)}{2\pi\kappa}.$$

Substituting all these dependencies with q_a into Eq. (12) provides the system of linear algebraic equations for the subweights C_{ina}, where indices j and a range from 1 to N_p and index m ranges from $-\infty$ to $+\infty$ excluding $m = 0$:

$$\begin{gathered} \sum_{i=1}^{N_p} \sum_{n=-\infty}^{\infty} C_{ina} \mathcal{F}'_{inj0} = 0 \\ \sum_{i=1}^{N_p} \sum_{n=-\infty}^{\infty} C_{ina} \left[\mathcal{F}_{injm} - \kappa \mathrm{R}_{pj} \mathcal{F}'_{injm} \right] = - \left[\mathcal{P}_{jma} - \kappa \mathrm{R}_{pj} \mathcal{P}'_{jma} \right]. \end{gathered} \tag{20}$$

Once the subweights C_{ina}, which do not depend on time, are known, the endogenous first-order corrections $\Theta^{(1)}_{j,\mathrm{en}}(\tau)$ for the fluid temperatures in the pipes can be obtained from Eq. (13):

$$\sum_{i=1}^{N_p} \sum_{n=-\infty}^{\infty} \sum_{a=1}^{N_p} C_{ina} \left[\mathcal{F}_{inj0} - \kappa \mathrm{R}_{pj} \mathcal{F}'_{inj0} \right] \frac{\mathrm{q}_a(\tau)}{2\pi\kappa} = \Theta^{(1)}_{j,\mathrm{en}}(\tau) - \sum_{a=1}^{N_p} \left[\mathcal{P}_{j0a} - \kappa \mathrm{R}_{pj} \mathcal{P}'_{j0a} \right] \frac{\mathrm{q}_a(\tau)}{2\pi\kappa}.$$

4.3.1. Network of thermal resistances

Previous expression can be conveniently reinterpreted as a network of thermal resistances, leading to the mathematically equivalent expression

$$\sum_{j=1}^{N_p} \hat{\mathrm{R}}^{(1)}_{ij} \mathrm{q}_j(\tau) = \Theta^{(1)}_{i,\mathrm{en}}(\tau).$$

Since the endogenous first-order problem is characterized by the absence of constraints imposed by the outer region on the inner region, no apparent ground temperature appears on the right-hand side of the expression.

The first-order corrections $\hat{\mathrm{R}}^{(1)}_{ij}$ to the thermal resistances, which are time-independent, are given by

$$2\pi\kappa \hat{\mathrm{R}}^{(1)}_{ij} = \sum_{a=1}^{N_p} \sum_{n=-\infty}^{\infty} C_{anj} \left[\mathcal{F}_{ani0} - \kappa \mathrm{R}_{pi} \mathcal{F}'_{ani0} \right] + \left[\mathcal{P}_{i0j} - \kappa \mathrm{R}_{pi} \mathcal{P}'_{i0j} \right].$$

This expression can be simplified in two steps. First, as demonstrated in the Appendix, $\mathcal{P}'_{i0}(\tau) = 0$. Consequently, $\mathcal{P}'_{i0j} = 0$. Second, the first set of equations in Eq. (20) also applies. Therefore, the final expression for the first-order corrections to the thermal resistances is

$$2\pi\kappa \hat{\mathrm{R}}^{(1)}_{ij} = \sum_{a=1}^{N_p} \sum_{n=-\infty}^{\infty} C_{anj} \mathcal{F}_{ani0} + \mathcal{P}_{i0j}.$$

5. Apparent ground temperature

Each of the three problems solved in the previous section introduces a network of thermal resistances that links the specified heat injection rates per unit pipe length with the resulting fluid temperatures in the pipes and the apparent ground temperatures for these pipes. In this section, these results are combined to form a single network of thermal resistances that models the thermal interaction of geothermal boreholes with creeping groundwater flows.

The combination procedure aims to reconstruct the fluid temperatures in the pipes from their asymptotic constituents:

$$\Theta_i(\tau) = \Theta^{(0)}_i(\tau) + \mathrm{Pe} \left[\Theta^{(1)}_{i,\mathrm{ex}}(\tau) + \Theta^{(1)}_{i,\mathrm{en}}(\tau) \right].$$

Following this combination procedure, the resulting network of thermal resistances is obtained as follows:

$$\sum_{j=1}^{N_p} \hat{\mathrm{R}}_{ij} \mathrm{q}_j(\tau) = \Theta_i(\tau) - \Theta_{ai}(\tau), \tag{21}$$

in which thermal resistances $\hat{\mathrm{R}}_{ij}$ and apparent ground temperatures for the pipes $\Theta_{ai}(\tau)$ are given by

$$\begin{aligned} \hat{\mathrm{R}}_{ij} &= \hat{\mathrm{R}}^{(0)}_{ij} + \mathrm{Pe}\, \hat{\mathrm{R}}^{(1)}_{ij} \\ \Theta_{ai}(\tau) &= \Theta^{(0)}_{ai}(\tau) + \mathrm{Pe}\, \Theta^{(1)}_{ai}(\tau). \end{aligned} \tag{22}$$

5.1. Single borehole

Next, the case of a single borehole is considered to obtain more specific expressions for the apparent ground temperatures of the pipes. The goal is to use these expressions in a forthcoming section to assess the merits and limitations of the state of the art.

To derive these expressions, values for $A(\tau)$, $B(\tau)$, and $C(\tau)$ are required. These are obtained from the study of the outer region in the thermal interaction of single geothermal boreholes with creeping groundwater flows [27]. In that work, the Laplace transform is used to address the time dependence of the problem [64], providing expressions for the Laplace transforms of $A(\tau)$, $B(\tau)$, and $C(\tau)$. In the following, a tilde ($\sim$) denotes the Laplace-transformed variable, and s represents the position in the complex-valued Laplace plane.

By comparing the matching condition, Eq. (4), with the work done by the authors [27], the following expressions result for the Laplace transforms of $A(\tau)$, $B(\tau)$, and $C(\tau)$:

$$\tilde{A}(s) = -\frac{\tilde{q}(s)}{2\pi}\left[\ln\left(\frac{Pe}{4}\sqrt{1+\frac{4s}{Pe^2}}\right)+\gamma\right]$$

$$\tilde{B}(s) = \frac{\tilde{A}_{0(+1)}(s)+\tilde{A}_{0(-1)}(s)}{2}\left[\ln\left(\frac{Pe}{4}\sqrt{1+\frac{4s}{Pe^2}}\right)+\gamma+\frac{1}{2}\right]$$

$$\tilde{C}(s) = -\frac{\tilde{q}(s)}{8\pi}\left[\ln\left(\frac{Pe}{4}\sqrt{1+\frac{4s}{Pe^2}}\right)+\gamma\right].$$

In these expressions, γ represents Euler's constant, $\tilde{q}(s)$ denotes the Laplace transform of the heat injection rate per unit borehole length, given by

$$\tilde{q}(s) = \sum_{j=1}^{N_p}\tilde{q}_j(s),$$

and $\tilde{A}_{0(\pm1)}(s)$ stands for the Laplace transforms of the first harmonics of the Fourier series expansion of the grout/ground temperature around the borehole wall:

$$\tilde{A}_{0(\pm1)}(s) = \sum_{a=1}^{N_p} A_{0(\pm1)a}\frac{\tilde{q}_a(s)}{2\pi\kappa}.$$

5.1.1. Time-domain recovery

To retrieve the time evolution of the problem, the inverse Laplace transform needs to be applied to the previous expressions for $\tilde{A}(s)$, $\tilde{B}(s)$, and $\tilde{C}(s)$. Generally, performing the inverse Laplace transform cannot be achieved analytically and requires numerical methods instead [65]. Fortunately, this is not necessary in this context, as an exact inversion is feasible, leveraging the known Laplace transform of the exponential integral $E_1(z)$ [66]:

$$\mathcal{L}\left[E_1\left(\frac{Pe^2}{4}\tau\right)\right] = \frac{\ln\left(1+\frac{4s}{Pe^2}\right)}{s}.$$

The Laplace inversion will be detailed for $\tilde{A}(s)$, with the inversion of $\tilde{B}(s)$ and $\tilde{C}(s)$ following identical procedures. Firstly, $\tilde{A}(s)$ must be reformulated to resemble the aforementioned Laplace transform of the exponential integral. Then, the initial value $q(0)$ for the heat injection rate per unit borehole length is both added and subtracted strategically to construct the Laplace transform of the time derivative of $q(\tau)$. The outcome is

$$\tilde{A}(s) = -\frac{\tilde{q}(s)\,s - q(0)}{4\pi}\frac{\ln\left(1+\frac{4s}{Pe^2}\right)+\ln\left(\frac{Pe^2}{16}\right)+2\gamma}{s} - \frac{q(0)}{4\pi}\frac{\ln\left(1+\frac{4s}{Pe^2}\right)+\ln\left(\frac{Pe^2}{16}\right)+2\gamma}{s}.$$

Thanks to the convolution theorem or integral [64], obtaining the inverse Laplace transform of the previous expression is straightforward:

$$A(\tau) = -\frac{1}{4\pi}\int_0^\tau \frac{dq}{d\lambda}\left[E_1\left(\frac{Pe^2}{4}(\tau-\lambda)\right)+\ln\left(\frac{Pe^2}{16}\right)+2\gamma\right]d\lambda - \frac{q(0)}{4\pi}\left[E_1\left(\frac{Pe^2}{4}\tau\right)+\ln\left(\frac{Pe^2}{16}\right)+2\gamma\right].$$

Upon integration by parts, this yields the sought result for $A(\tau)$:

$$A(\tau) = -\frac{q(\tau)}{4\pi}\left[E_1\left(\frac{Pe^2}{4}\tau\right)+\ln\left(\frac{Pe^2}{16}\right)+2\gamma\right] - \frac{1}{4\pi}\int_0^\tau \frac{q(\tau)-q(\lambda)}{\tau-\lambda}e^{-\frac{Pe^2}{4}(\tau-\lambda)}d\lambda.$$

To facilitate the outcome of the Laplace inversion of $\tilde{B}(s)$, it is more convenient to express it in combination with $A(\tau)$ as follows:

$$A(\tau)+Pe\,B(\tau) = -\frac{f(\tau)}{4\pi}\left[E_1\left(\frac{Pe^2}{4}\tau\right)+\ln\left(\frac{Pe^2}{16}\right)+2\gamma\right] - \frac{1}{4\pi}\int_0^\tau \frac{f(\tau)-f(\lambda)}{\tau-\lambda}e^{-\frac{Pe^2}{4}(\tau-\lambda)}d\lambda + Pe\frac{A_{0(+1)}(\tau)+A_{0(-1)}(\tau)}{4}.$$

This combination highlights the emergence of the fictitious heat injection rate per unit borehole length $f(\tau)$ in the expression:

$$f(\tau) = q(\tau) - Pe\,\pi\left(A_{0(+1)}(\tau)+A_{0(-1)}(\tau)\right).$$

This quantity is identical to that present in the solution to the outer region found in the literature [27]. This consistency is expected, as the outer solution needs to be expanded close to the borehole to perform its asymptotic matching with the inner solution.

Lastly, the Laplace inversion of $\tilde{C}(s)$ yields the following expression for $C(\tau)$:

$$C(\tau) = -\frac{q(\tau)}{16\pi}\left[E_1\left(\frac{Pe^2}{4}\tau\right)+\ln\left(\frac{Pe^2}{16}\right)+2\gamma\right] - \frac{1}{16\pi}\int_0^\tau \frac{q(\tau)-q(\lambda)}{\tau-\lambda}e^{-\frac{Pe^2}{4}(\tau-\lambda)}d\lambda.$$

As anticipated in Section 2.4.1, for a single borehole interacting with a groundwater stream, the temperature gradient imposed by the outer region onto the inner region aligns perfectly with the flow direction, resulting in $C(\tau)$ being real-valued.

5.1.2. Constant heat injection rates

When heat injection rates per unit pipe length remain constant over time, $f(\tau)$ and $A_{0(\pm1)}(\tau)$ also become constants, leading to a significant simplification of the previous expressions for $A(\tau)$, $B(\tau)$, and $C(\tau)$. Specifically, for $A(\tau)$ and $B(\tau)$,

$$A(\tau)+Pe\,B(\tau) = -\frac{f}{4\pi}\left[E_1\left(\frac{Pe^2}{4}\tau\right)+\ln\left(\frac{Pe^2}{16}\right)+2\gamma\right] + Pe\frac{A_{0(+1)}+A_{0(-1)}}{4}, \tag{23}$$

while for $C(\tau)$ the simplification leads to

$$C(\tau) = -\frac{q}{16\pi}\left[E_1\left(\frac{Pe^2}{4}\tau\right)+\ln\left(\frac{Pe^2}{16}\right)+2\gamma\right]. \tag{24}$$

Over time, $A(\tau)$, $B(\tau)$, and $C(\tau)$ gradually approach steady-state values, which can be computed from the previous expressions by allowing τ to tend to infinity:

$$\left[A+Pe\,B\right]_{\tau\to\infty} = -\frac{f}{4\pi}\left[\ln\left(\frac{Pe^2}{16}\right)+2\gamma\right]+Pe\frac{A_{0(+1)}+A_{0(-1)}}{4}$$

$$C\Big|_{\tau\to\infty} = -\frac{q}{16\pi}\left[\ln\left(\frac{Pe^2}{16}\right)+2\gamma\right].$$

For non-zero Peclet numbers, steady-state values are always attained, as indicated by the expressions just presented. However, when the Peclet number is zero, no steady-state is achieved due to the divergent behavior of these expressions when $Pe = 0$. The absence of a steady-state solution under these conditions is not surprising and is well documented and explained in the literature [27,67].

5.1.3. Purely conductive limit

For completeness, the present section recovers the purely conductive limit from the results presented thus far. As the Peclet number tends to zero, the first-order correction to the apparent ground temperatures for the pipes disappears, leaving only the zeroth-order values $\Theta_{ai}^{(0)}(\tau)$ intact. Therefore, only $A(\tau)$ is relevant in the purely conductive limit. Computing its behavior as the Peclet number tends to zero yields the following result for the apparent ground temperatures for the pipes:

$$\Theta_{ai}(\tau)\Big|_{Pe\to0} = \frac{q(\tau)}{4\pi}[\ln(4\tau)-\gamma] - \frac{1}{4\pi}\int_0^\tau \frac{q(\tau)-q(\lambda)}{\tau-\lambda}d\lambda.$$

This expression matches the one found in the literature for the apparent temperature of purely conductive grounds [17,41].

6. Borehole thermal resistances

Next, the impact of a groundwater stream on the thermal resistances of the borehole is analyzed. In the literature on purely conductive grounds, it is common practice to invert the network of thermal resistances. This inversion allows for explicit expression of the heat injection rates per unit pipe length in terms of fluid temperatures and the apparent ground temperature [16,17,36,41].

Proceeding similarly with Eq. (21) leads to

$$\mathrm{q}_i(\tau) = \sum_{j=1}^{N_p} \frac{\Theta_j(\tau) - \Theta_{aj}(\tau)}{\mathrm{R}_{ij}}, \tag{25}$$

where the thermal resistances R_{ij} are defined as in Rivero and Hermanns (2021) [41]:

$$\begin{bmatrix} \frac{1}{\mathrm{R}_{11}} & \frac{1}{\mathrm{R}_{12}} & \cdots \\ \frac{1}{\mathrm{R}_{21}} & \frac{1}{\mathrm{R}_{22}} & \cdots \\ \vdots & \vdots & \ddots \end{bmatrix} = \begin{bmatrix} \hat{\mathrm{R}}_{11} & \hat{\mathrm{R}}_{12} & \cdots \\ \hat{\mathrm{R}}_{21} & \hat{\mathrm{R}}_{22} & \cdots \\ \vdots & \vdots & \ddots \end{bmatrix}^{-1}.$$

Eq. (25) is typically reformulated in a more insightful manner, as detailed in the literature [41]. Applying the same steps and concepts to the present problem, where different apparent ground temperatures are defined for each pipe, leads to

$$\mathrm{q}_i(\tau) = w_i \frac{\Theta_m(\tau) - \Theta_a(\tau)}{\mathrm{R}_b} + \sum_{j=1}^{N_p} \frac{\big(\Theta_i(\tau) - \Theta_{ai}(\tau)\big) - \big(\Theta_j(\tau) - \Theta_{aj}(\tau)\big)}{\mathrm{R}_{a,ij}}. \tag{26}$$

Most quantities are defined as in the existing literature for purely conductive grounds [41]. Thus, the borehole's outer thermal resistance, R_b, which governs the overall heat exchange between the borehole and the ground, is defined as:

$$\frac{1}{\mathrm{R}_b} = \sum_{i=1}^{N_p} \sum_{j=1}^{N_p} \frac{1}{\mathrm{R}_{ij}}.$$

The primary weighting coefficients w_i, which represent the contribution of each pipe to the overall heat exchange between the borehole and the ground, are defined as

$$\frac{w_i}{\mathrm{R}_b} = \sum_{j=1}^{N_p} \frac{1}{\mathrm{R}_{ij}} \qquad \text{with} \qquad \sum_{i=1}^{N_p} w_i = 1.$$

The weighted mean fluid temperature $\Theta_m(\tau)$, representing the temperature at which the borehole exchanges heat with the ground, is defined as

$$\Theta_m = \sum_{j=1}^{N_p} v_j \Theta_j,$$

with the contribution of each pipe specified by the secondary weighting coefficients v_j:

$$\frac{v_j}{\mathrm{R}_b} = \sum_{i=1}^{N_p} \frac{1}{\mathrm{R}_{ij}} \qquad \text{with} \qquad \sum_{j=1}^{N_p} v_j = 1.$$

The borehole's inner thermal resistances $\mathrm{R}_{a,ij}$, which govern the heat exchange between pairs of pipes within the borehole, are also defined as in the existing literature for purely conductive grounds,

$$\frac{1}{\mathrm{R}_{a,ij}} = \frac{w_i v_j}{\mathrm{R}_b} - \frac{1}{\mathrm{R}_{ij}},$$

with the complete set of inner thermal resistances satisfying the following relationship, which is necessary, among other things, for the recasting of Eq. (25) into Eq. (26):

$$\sum_{i=1}^{N_p} \frac{1}{\mathrm{R}_{a,ij}} = \sum_{j=1}^{N_p} \frac{1}{\mathrm{R}_{a,ij}} = 0. \tag{27}$$

A completely new concept introduced here for the first time is the weighted apparent ground temperature $\Theta_a(\tau)$, which represents the temperature at which the borehole as a whole perceives the surrounding ground:

$$\Theta_a = \sum_{j=1}^{N_p} v_j \Theta_{aj}.$$

The physical meaning of this concept becomes clear by summing the equations for all pipes in Eq. (26). This summation results in the heat injection rate per unit borehole length $\mathrm{q}(\tau)$ on the left-hand side, while several terms on the right-hand side cancel out due to Eq. (27):

$$\mathrm{q} = \frac{\Theta_m - \Theta_a}{\mathrm{R}_b}. \tag{28}$$

In this context, Θ_m is the temperature with which the borehole exchanges heat with the ground, Θ_a is the temperature at which the borehole perceives the surrounding ground, and R_b is the thermal resistance governing the overall heat exchange between the borehole and the ground.

In addition to introducing the weighted apparent ground temperature Θ_a, another difference arises in contrast to the state of the art, as Eq. (26) also includes the apparent ground temperatures Θ_{ai} in the rightmost terms representing the heat exchange between pipes. This distinction emphasizes that the excess temperature of the fluid in each pipe, relative to its apparent ground temperature, is the critical factor in the heat exchange between pipes, rather than the fluid temperature itself.

7. Numerical examples

To evaluate the impact of creeping groundwater flows on the apparent ground temperatures for the pipes and the borehole's thermal resistances and weighting coefficients, this section numerically solves the systems of linear algebraic equations outlined in Eqs. (17)–(20). Given that these systems entail an infinite number of equations, indexes n and m must be truncated, introducing truncation errors into the results. Thankfully, the spectral convergence of the enhanced multipole method [41] ensures that these errors diminish rapidly with the number of multipoles retained in the expansion of the grout/ground temperature. Hence, limiting n and m to values between −20 and +20 already guarantees an accuracy level surpassing the requirements of the present work.

7.1. Borehole description

All comparisons and discussions in the subsequent subsections are based on the borehole configuration depicted in Fig. 2. Although other borehole configurations with varying geometrical and thermal characteristics, including coaxial probes, have been examined, their results are not included here as they align with what is presented.

The selected configuration, adopted from the literature [27], comprises a borehole with a diameter of $2r_b = 152\,\mathrm{mm}$ housing a single U-shaped probe with heterogeneous properties. The first pipe of the probe has an outer diameter of $2r_{p1} = 40\,\mathrm{mm}$ and a wall thickness of $d_1 = 3.7\,\mathrm{mm}$, while the second pipe has an outer diameter of $2r_{p2} = 50\,\mathrm{mm}$ and a wall thickness of $d_2 = 4.6\,\mathrm{mm}$. Positioned 5 mm from the borehole wall, the two pipes are oriented at ±45° from the rear stagnation point, resulting in their center coordinates being (51 mm, +45°) and (46 mm, −45°), respectively.

The space between the pipes and the ground, with an effective thermal conductivity $k_g = 3.00\,\mathrm{W/(m\,K)}$ and effective thermal diffusivity $\alpha_g = 2.24 \cdot 10^{-7}\,\mathrm{m^2/s}$ [4], is filled with conventional grout having a thermal conductivity $k_b = 1.50\,\mathrm{W/(m\,K)}$ [68].

Pure water serves as heat carrying liquid. Its density, specific heat capacity, thermal conductivity, and dynamic viscosity are $999\,\mathrm{kg/m^3}$, $4184\,\mathrm{J/(kg\,K)}$, $0.577\,\mathrm{W/(m\,K)}$, and $1.138 \cdot 10^{-3}\,\mathrm{kg/(m\,s)}$, respectively. A

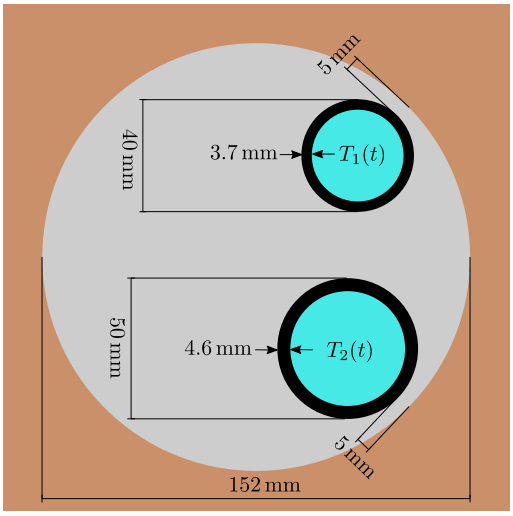

Fig. 2. Borehole configuration for the numerical examples.

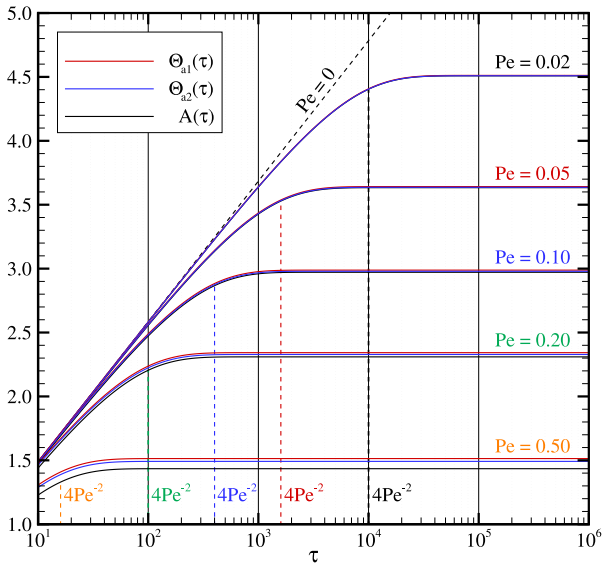

Fig. 3. Time evolution of the apparent ground temperatures for the pipes $\Theta_{ai}(\tau)$ for different Peclet numbers of the groundwater flow.

turbulent flow regime is maintained in both pipes due to a pumped mass flow rate of 0.25 kg/s, with turbulent heat transport inside the liquid modeled using convective heat transfer coefficients h_1 and h_2, determined using Gnielinski's correlations [69]. Together with the thermal conductivities of the pipes $k_1 = k_2 = 0.42\,\mathrm{W/(m\,K)}$, the following inner thermal resistances for the pipes result:

$$R_{p1} = 0.535\,\frac{\mathrm{m\,K}}{\mathrm{W}}, \qquad R_{p2} = 0.544\,\frac{\mathrm{m\,K}}{\mathrm{W}}.$$

In all results presented in the subsequent sections, time-constant non-dimensional heat injection rates per unit pipe length are specified for the pipes, such that $q_1(\tau) = 5$ and $q_2(\tau) = 1$.

7.2. Apparent ground temperatures

The first quantities under scrutiny are the apparent ground temperatures for the two pipes, $\Theta_{a1}(\tau)$ and $\Theta_{a2}(\tau)$. Fig. 3 illustrates their temporal evolution alongside the apparent ground temperature employed by the state of the art. That is, $\Theta_{ai}^{(0)}(\tau) = A(\tau)$. Initially, a uniform logarithmic growth is observed across all depicted temperatures and for all considered Peclet numbers of the groundwater flow. This shared behavior ceases once the system reaches the steady-state discussed in Section 5.1.2. The transition between these behaviors occurs at non-dimensional times $\tau \sim 4\mathrm{Pe}^{-2}$, where the argument of the exponential integral E_1 in Eqs. (23) and (24) becomes of order unity.

The attained steady-state value is influenced by the Peclet number of the groundwater flow, with smaller Peclet numbers yielding higher steady-state values. Notably, in the absence of groundwater flows, no steady state is reached, as previously noted in Section 5.1.2. This scenario of zero Peclet number is depicted in Fig. 3 by an oblique dashed line.

Examining individual pipes, differences in their apparent ground temperatures arise solely from the first-order corrections $\Theta_{ai}^{(1)}(\tau)$. Generally, these differences are marginal, reflecting the similarity between the two pipes. However, significantly larger differences may arise when considering highly dissimilar pipes or assigning heat injection rates of opposite signs to the pipes. Yet, these scenarios are too divergent from reality to be practically meaningful.

Of greater significance is the disparity between the two pipes and the apparent ground temperature used by the state of the art, $A(\tau)$. For small Peclet numbers, this difference is minimal, rendering $A(\tau)$ sufficiently accurate. However, as the Peclet number increases, so does the difference, reaching 5.5% for Pe = 0.5. Such elevated Peclet numbers are indeed encountered in real-world installations, particularly in settings involving unconsolidated grounds or energy piles [70].

The first-order correction, responsible for these discrepancies, also reveals a novel phenomenon. In the zeroth-order solution, equivalent to the state of the art, the borehole's orientation is irrelevant, as the outer region imposes a uniform temperature level $A(\tau)$ onto the inner region. Consequently, all pipes perceive the same apparent ground temperature $\Theta_{ai}^{(0)}(\tau) = A(\tau)$, ignoring their position within the borehole. However, with the first-order correction, the outer region enforces a temperature gradient onto the inner region. This spatial gradient, combined with the pipes' positions within the borehole, leads to apparent ground temperatures that vary based on the borehole's orientation relative to the groundwater flow.

To illustrate this phenomenon, four different borehole orientations are analyzed next. In addition to the original orientation depicted in Fig. 2, three counterclockwise rotations of 90°, 180°, and 270° are considered. As shown in Fig. 4, varying borehole orientations result in distinct weighted apparent ground temperatures. For Pe = 0.5, for example, a variation of 15.2% exists between the 90° rotation, where $\Theta_a(\tau)$ reaches its peak, and the 270° rotation, where $\Theta_a(\tau)$ is at its lowest.

Given that the weighted apparent ground temperature reflects how the borehole as a whole perceives the surrounding ground, the observed variations in $\Theta_a(\tau)$ translate to differing heat exchanges between the borehole and the ground. However, capitalizing on this effect in real-world installations is challenging, as there is no control over the positioning of pipes within the borehole during construction, resulting in arbitrary variations in pipe positions with depth.

7.3. Borehole thermal resistances and weights

The first thermal resistance to analyze is the borehole's inner thermal resistance $R_{a,12}$. As elaborated in Section 6, this thermal resistance dictates the heat transfer between the two pipes. Its expected dependence with the Peclet number of the groundwater flow can be deduced from its expression in terms of the thermal resistances $\hat{R}_{ij}$, which emerges from applying the formulas outlined in Section 6:

$$R_{a,12} = R_{a,21} = \hat{R}_{11} + \hat{R}_{22} - \hat{R}_{12} - \hat{R}_{21}.$$

Since the thermal resistances $\hat{R}_{ij}$ display linear variations with the Peclet number of the groundwater flow, as demonstrated in Eq. (22), it follows that the inner thermal resistance must exhibit a similar

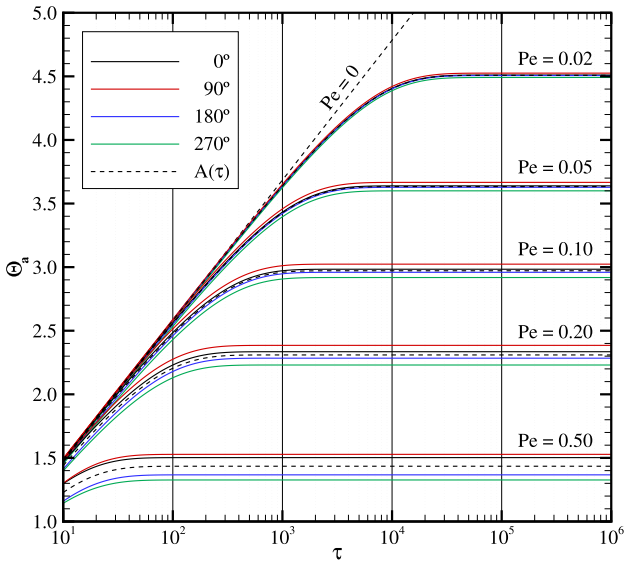

Fig. 4. Time evolution of the weighted apparent ground temperature $\Theta_a(\tau)$ for different Peclet numbers of the groundwater flow and for four different orientations of the borehole.

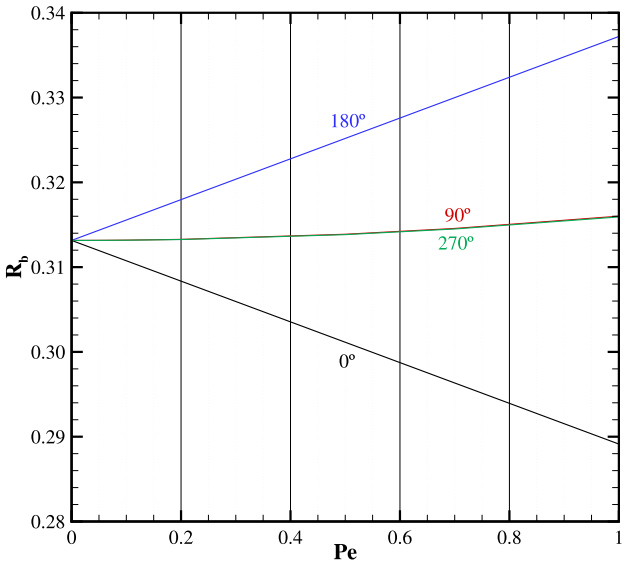

Fig. 5. Dependence of outer thermal resistance R_b on the Peclet number of the groundwater flow for four different orientations of the borehole.

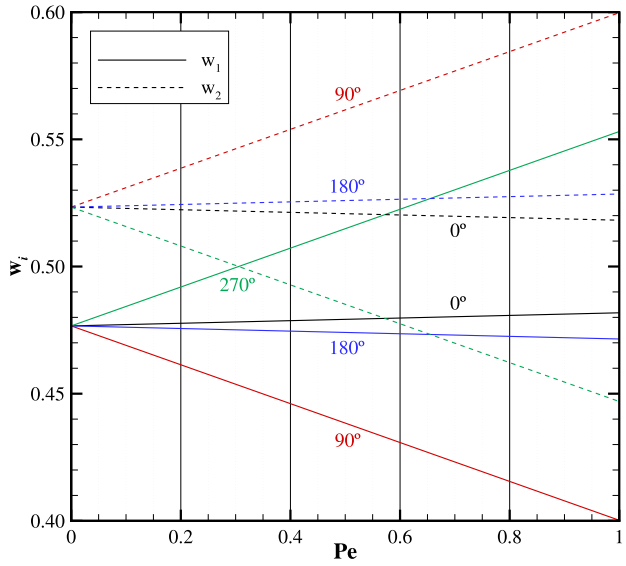

Fig. 6. Dependence of primary weighting coefficients w_i on the Peclet number of the groundwater flow for four different orientations of the borehole.

behavior. However, numerical findings indicate that its value remains constant, fixed at $R_{a,12} = 1.0996$, irrespective of the Peclet number of the groundwater flow. While most of the heat exchange between the two pipes occurs through the grout, the absence of any correlation with the groundwater motion around the borehole is unexpected. Further investigation is necessary to fully understand this phenomenon.

The next thermal resistance to consider is the borehole's outer thermal resistance R_b, which regulates the overall heat exchange between the borehole and the ground [41]. Fig. 5 illustrates its dependence with the Peclet number of the groundwater flow across the same four borehole orientations of the previous subsection. A clear dependence with the Peclet number is observed, leading to spreads of nearly 8% when the Peclet number reaches one. These substantial spreads are observed for borehole orientations where the pipes are positioned at the rear and front of the borehole, such as the original borehole configuration and its 180° rotation.

Given that R_b directly influences the overall heat exchange between the borehole and the ground, positioning the pipes at the back of the borehole, as depicted in Fig. 2, is optimal for enhancing this heat exchange. The advantage of this pipe placement over the others lies in the prompt removal of advected heat from the borehole. In contrast, in the other three locations, the supplied heat must initially circulate around the borehole, which disrupts the heat exchange at various points along the borehole wall. Unfortunately, capitalizing on this effect in real-world installations is challenging due to the unregulated positioning of pipes within boreholes.

The observed dependence of R_b on the Peclet number of the groundwater flow can be explained using the expression for R_b in terms of the thermal resistances $\hat{R}_{ij}$ derived from the formulae presented in Section 6:

$$R_b = \frac{\hat{R}_{11}\hat{R}_{22} - \hat{R}_{12}\hat{R}_{21}}{\hat{R}_{11} + \hat{R}_{22} - \hat{R}_{12} - \hat{R}_{21}}.$$

This expression shows a rational dependence where the numerator is a quadratic polynomial and the denominator is a linear polynomial in the Peclet number. Notably, the denominator coincides with the borehole's inner thermal resistance, which remains constant. As a result, the borehole's outer thermal resistance, R_b, exhibits a quadratic dependence on the Peclet number. This quadratic behavior is most evident for borehole orientations corresponding to rotations of 90° and 270°.

Finally, the primary and secondary weighting coefficients, w_i and v_j, are discussed. They represent the contribution of each pipe to the overall heat exchange between the borehole and the ground, and to the weighted mean fluid temperature, respectively [41]. In the absence of thermal inertia in the grout and ground, these weighting coefficients are identical, and no distinction is made between them [71]. However, this equivalence applies only to purely conductive grounds. In the present case, the coefficients differ, though the discrepancies are small, within the range of 0.1% for the considered borehole configuration. Therefore, only the primary weighting coefficients w_i will be discussed next.

Fig. 6 depicts the primary weighting coefficients for the two pipes, w_1 and w_2, as functions of the Peclet number of the groundwater flow, considering the four borehole orientations of interest. Due to the differences between the two pipes, their contributions to the overall heat exchange are unequal, with $w_1 = 0.477$ and $w_2 = 0.523$ in the absence of groundwater flow. When groundwater is in motion, the

primary weighting coefficients vary linearly with the Peclet number. This linear dependence can be explained using the expressions for w_i derived from the formulae presented in Section 6:

$$w_1 = \frac{\hat{R}_{22} - \hat{R}_{12}}{\hat{R}_{11} + \hat{R}_{22} - \hat{R}_{12} - \hat{R}_{21}}, \qquad w_2 = \frac{\hat{R}_{11} - \hat{R}_{21}}{\hat{R}_{11} + \hat{R}_{22} - \hat{R}_{12} - \hat{R}_{21}}.$$

Since the denominators coincide with the invariant borehole's inner thermal resistance $R_{a,12}$, the linear dependence of the numerators on the Peclet number explains the overall linear relationship.

The most interesting borehole orientations to discuss are those corresponding to rotations of 90° and 270°. For both orientations, the influence of the Peclet number is the highest, consistently increasing the heat exchange of the downstream pipe while decreasing that of the upstream pipe. For example, at Pe = 1 with a 90° rotation of the original borehole, pipe 2's contribution increases by 14.6%, while pipe 1's contribution decreases accordingly. When the borehole is rotated 270°, this trend reverses: pipe 1's contribution increases by 16%, and pipe 2's contribution decreases accordingly. As shown in Fig. 6, these significant changes in the primary weighting coefficients result in an inversion of the pipes' relevance for Peclet numbers greater than 0.30.

For the sake of completeness, expressions for the secondary weighting coefficients v_j are also provided. These are derived from the formulae presented in Section 6:

$$v_1 = \frac{\hat{R}_{22} - \hat{R}_{21}}{\hat{R}_{11} + \hat{R}_{22} - \hat{R}_{12} - \hat{R}_{21}}, \qquad v_2 = \frac{\hat{R}_{11} - \hat{R}_{12}}{\hat{R}_{11} + \hat{R}_{22} - \hat{R}_{12} - \hat{R}_{21}}.$$

7.4. Weighted mean fluid temperature

The thermal response of the borehole is characterized by the time evolution of its weighted mean fluid temperature, Θ_m. This temperature directly impacts the efficiency of the heat pump driving the geothermal installation, as its coefficient of performance (COP) depends on the temperature of the heat-carrying liquid.

Fig. 7 illustrates the time evolution of the weighted mean fluid temperature for different Peclet numbers of the groundwater flow and the four borehole orientations considered thus far. Overall, the behavior of Θ_m closely mirrors that of the weighted apparent ground temperature Θ_a. This similarity is expected, given the tight relationship between the two temperatures as described in Eq. (28).

As observed in previous results, the orientation of the borehole plays a secondary role at low Peclet numbers of the groundwater flow. However, its influence becomes more significant with increasing Peclet numbers. For instance, the difference in Θ_m between the best and worst performing borehole orientations reaches 6.3% for Pe = 0.5. This is less than half of the previously reported relative difference in the weighted apparent ground temperature, a direct consequence of the larger values attained by Θ_m compared to Θ_a.

7.5. Fluid temperatures

The present work builds on the asymptotic analysis of the thermal interaction of geothermal boreholes with creeping groundwater flows [27]. By retaining terms beyond the zeroth-order, the authors have advanced the state of the art in understanding of the problem and numerical accuracy of the results.

This study, with its mathematically exact derivation of the zeroth-order solution and first-order correction to the inner region, shares the benefits of the underlying asymptotic analysis. However, assessing the accuracy of the quantities introduced here (Θ_{ai}, Θ_a, R_b, $R_{a,ij}$, w_i, v_j, and Θ_m) is impossible since their very definitions are based on the developed theory. Thus, their numerical values cannot be independently computed, which is essential for any accuracy assessment.

The same challenge arises when determining the range of validity of the developed theory, specifically identifying the Peclet number values beyond which the underlying asymptotic analysis, and consequently the results of this work, become invalid. To address this limitation, fluid temperatures in the pipes, Θ_i, are used for this determination. These values can be obtained from both the developed model and detailed numerical simulations of the complete heat transfer problem. Full details regarding the complete heat transfer problem and its numerical solution can be found in Rico and Hermanns (2024) [27].

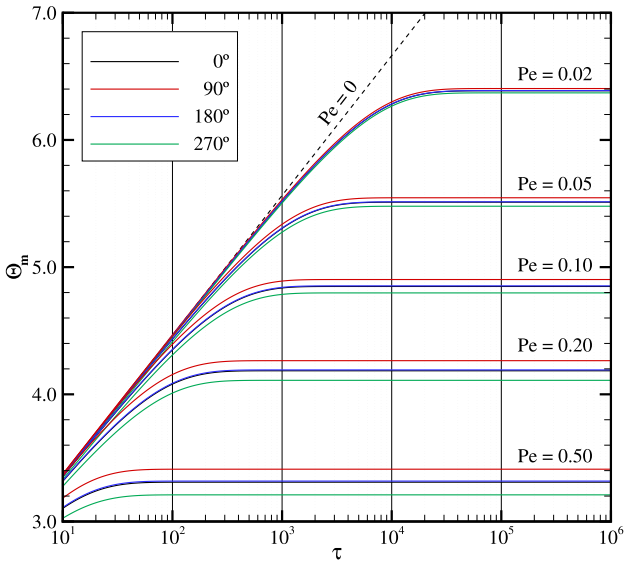

Fig. 7. Time evolution of the weighted mean fluid temperature $\Theta_m(\tau)$ for different Peclet numbers of the groundwater flow and for four different orientations of the borehole.

Fig. 8 shows the steady-state fluid temperatures Θ_1 and Θ_2, attained as τ tends to infinity, as functions of the Peclet number of the groundwater flow and for the four borehole orientations considered in previous subsections. For Peclet numbers of order 10^{-1} and below, the differences between the developed model and the reference solution are small. However, errors become significant for Peclet numbers of order unity, clearly restricting the validity of the developed model to creeping groundwater flows.

The results shown in Fig. 8 indicate three key points. First, the developed model works well for creeping groundwater flows, performing better than the state of the art, which cannot capture the influence of the borehole's orientation (The state-of-the-art results are not shown in the figure as they overlap with those of the developed model for the original borehole orientation). Second, the influence of the borehole's orientation is strong for Peclet numbers of order unity, regardless of the developed model's performance. This leads to the third point: a model specifically tailored for Peclet numbers of order unity is required to address the needs of energy piles and boreholes constructed in strongly fractured or unconsolidated grounds [70].

8. Conclusions

The presence of aquifers in the ground significantly impacts the thermal response of geothermal boreholes. To account for this during the design stages of a geothermal HVAC system, theoretical models are required to accurately represent the mechanical and thermal interactions between geothermal boreholes and groundwater flows. Such models already exist in the literature and adapt concepts, ideas, and procedures designed for purely conductive grounds to address these interactions.

While existing models perform reasonably well, the approach of *"adopting what is done for purely conductive grounds"* leads to theoretical inconsistencies and overlooks interesting and/or relevant phenomena introduced by aquifers. To overcome these limitations, a mathematically rigorous derivation of a physically sound model is necessary. The

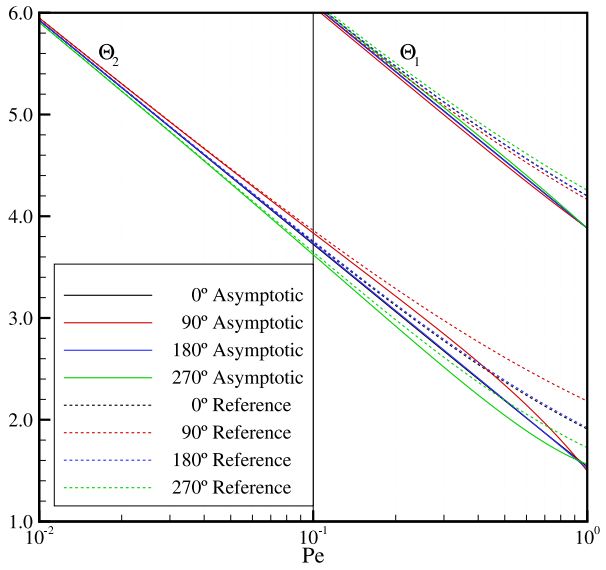

Fig. 8. Steady-state fluid temperatures Θ_1 and Θ_2 as functions of the Peclet number of the groundwater flow and for four different orientations of the borehole.

present work, along with another manuscript recently published by the authors, addresses this need specifically for creeping groundwater flows, where the Peclet number of the flow is small compared to unity.

The previous work by the authors dissected the overall heat transfer problem using asymptotic expansion techniques, identifying the existence of two distinct regions and formulating the mathematical problems to solve in each region. In contrast, the present work focuses entirely on the inner region, encompassing the borehole, its pipes and grout, and the ground located close to the borehole.

To obtain exact, rather than numerical, solutions to the formulated problems in the inner region, the present work has modified the enhanced multipole method to address new phenomena introduced by the aquifer. These phenomena include the spatial temperature gradient enforced by the outer region on the inner region and the weak convective transport of heat in the vicinity of the borehole.

Through the precise manipulation and combination of the resulting solutions, a network of thermal resistances has been established. This network represents an exact relationship between the heat injection rates per unit length of the pipes, fluid temperatures in the pipes, and apparent ground temperatures for the pipes, with thermal resistances serving as the proportionality constants.

Compared to the state of the art, which also utilizes a similar network of thermal resistances, two important differences emerge. First, each pipe perceives the surrounding ground at a different apparent ground temperature, whereas the state of the art assumes a uniform apparent ground temperature for all pipes. This difference arises from the temperature gradient enforced by the outer region on the inner region, originating from the flowing aquifer. Second, the thermal resistances depend on the Peclet number of the groundwater flow, while in the state of the art their values are constant. This change results as the state of the art neglects the weak convective transport of heat in the vicinity of the borehole.

In addition to uncovering these theoretical inconsistencies, the present work also assesses the accuracy of the state of the art using the newly developed model as a benchmark. For creeping groundwater flows, accuracy is not affected by the identified inconsistencies, explaining why the state of the art performs well. However, for larger Peclet numbers, significant discrepancies are observed. Variations of up to 15% exist in the apparent ground temperatures for the pipes, and changes of up to 8% are reported for the thermal resistances.

Although this work shows that the identified discrepancies worsen with increasing Peclet numbers, no confident conclusion regarding their real magnitude and relevance can be drawn since the validity and accuracy of the developed asymptotic model are not assured for such large Peclet numbers. Therefore, the rigorous development of a theoretical model for the thermal interaction of geothermal boreholes with strong groundwater flows is the target of future work.

CRediT authorship contribution statement

Javier Rico: Writing – review & editing, Writing – original draft, Validation, Software, Formal analysis. **Miguel Hermanns:** Writing – review & editing, Writing – original draft, Visualization, Supervision, Methodology, Funding acquisition, Formal analysis, Conceptualization.

Declaration of competing interest

The authors declare that they have no known competing financial interests or personal relationships that could have appeared to influence the work reported in this paper.

Data availability

Data will be made available on request.

Acknowledgments

Grant PID2021-128172OB-I00 funded by MCIN/AEI/10.13039/501100011033 and by “ERDF A way of making Europe”.

Appendix. Endogenous particular solution

The solution to the endogenous first-order problem necessitates, as an intermediate stage, determining the particular solution Θ_p to the problem outlined in Table 2. This particular solution encompasses all the forcing terms of the governing equation in the ground and all the terms imposed by the inner region on the outer region. Subsequent subsections detail the steps involved in obtaining the aforementioned particular solution. Additionally, the coefficients $\mathcal{P}_{jm}$ and $\mathcal{P}'_{jm}$ of the Fourier series expansions around pipe j for Θ_p and its derivative with respect to ρ_j are determined.

A.1. Particular solution to ground equation

First, a particular solution Θ_g to the governing equation in the ground is proposed. It must also include all terms imposed by the inner region onto the outer region, which is not a challenging task as they are closely related to the forcing terms of the governing equation in the ground:

$$\begin{aligned}\Theta_g(\rho_0,\theta_0,\tau) = {} & \frac{\mathrm{A}_{0(+1)}(\tau)+\mathrm{A}_{0(-1)}(\tau)}{2}\ln\rho_0 \\ & - \frac{\mathrm{q}(\tau)}{4\pi}\left(\rho_0+\frac{1}{\rho_0}\right)\ln\rho_0\cos\theta_0 \\ & + \sum_{\substack{m=-\infty \\ m\neq 0}}^{\infty}\frac{\mathrm{A}_{0m}(\tau)}{4}\left[\frac{\mathrm{e}^{\imath\frac{m}{|m|}(|m|+1)\theta_0}}{\rho_0^{|m|-1}}+\frac{\mathrm{e}^{\imath\frac{m}{|m|}(|m|-1)\theta_0}}{\rho_0^{|m|+1}}\right].\end{aligned} \tag{A.1}$$

This particular solution Θ_g is only valid in the ground. Consequently, it does not comply with the governing equation in the grout and the continuity conditions at the borehole wall. Thus, further work is required to obtain Θ_p.

A.2. Fourier expansion around the borehole wall

Next, Fourier series expansions around the borehole wall of Θ_g and its derivative with respect to ρ_0 are obtained. These are required to enforce the continuity conditions at the borehole wall and to extend Θ_g towards the interior of the borehole.

Following the definitions introduced in Section 3.2 and treating the borehole as pipe $j = 0$, as discussed in Section 3.6, the Fourier series expansions for Θ_g and its radial derivative with respect to ρ_0 are defined as

$$\Theta_g\Big|_{\rho_0=\rho_{p0}} = \sum_{\ell=-\infty}^{\infty} \mathcal{G}_{0\ell}\, \mathrm{e}^{\imath\ell\theta_0}$$

$$\rho_{p0}\frac{\partial\Theta_g}{\partial\rho_0}\Big|_{\rho_0=\rho_{p0}} = \sum_{\ell=-\infty}^{\infty} \mathcal{G}'_{0\ell}\, \mathrm{e}^{\imath\ell\theta_0}.$$

The expressions for $\mathcal{G}_{0\ell}$ and $\mathcal{G}'_{0\ell}$ are derived by comparing these Fourier series expansions with Eq. (A.1) and its derivative with respect to ρ_0, evaluated at the borehole wall. Thus, for $|\ell| > 1$, the corresponding Fourier series coefficients are

$$\mathcal{G}_{0\ell} = \frac{\mathrm{A}_{0(\ell+1)}(\tau) + \mathrm{A}_{0(\ell-1)}(\tau)}{4}$$

and

$$\mathcal{G}'_{0\ell} = -\frac{|\ell|}{\ell}(\ell+2)\frac{\mathrm{A}_{0(\ell+1)}(\tau)}{4} - \frac{|\ell|}{\ell}(\ell-2)\frac{\mathrm{A}_{0(\ell-1)}(\tau)}{4}.$$

For $\ell = \pm 1$, the expressions to use are

$$\mathcal{G}_{0(\pm1)} = \frac{\mathrm{A}_{0(\pm2)}(\tau)}{4} \quad \text{and} \quad \mathcal{G}'_{0(\pm1)} = -\frac{\mathrm{q}(\tau)}{4\pi} - \frac{3}{4}\mathrm{A}_{0(\pm2)}(\tau).$$

Finally, for $\ell = 0$,

$$\mathcal{G}_{00} = \frac{\mathrm{A}_{0(+1)}(\tau) + \mathrm{A}_{0(-1)}(\tau)}{4} \qquad \text{and} \qquad \mathcal{G}'_{00} = 0.$$

In addition to the expressions for the Fourier series coefficients, an important result of this subsection is that $\mathcal{G}_{0\ell}$ and $\mathcal{G}'_{0\ell}$ are linear combinations of the specified heat injection rates per unit pipe length $\mathrm{q}_j(\tau)$, owing to the inherent properties of all involved quantities.

A.3. Continuity at borehole wall

To enforce the continuity conditions at the borehole wall and extend the particular solution Θ_g to the interior of the borehole, homogeneous solutions to the governing equations in both the grout and ground must be added to Θ_g. This yields the following expression for Θ_p:

$$\Theta_p = \begin{cases} \displaystyle\sum_{\ell=-\infty}^{\infty} \mathcal{P}_{0\ell}\rho_0^{|\ell|}\mathrm{e}^{\imath\ell\theta_0} & \text{if } \rho_0 \le 1 \\ \displaystyle\sum_{\ell=-\infty}^{\infty} \mathcal{B}_{0\ell}\rho_0^{-|\ell|}\mathrm{e}^{\imath\ell\theta_0} + \Theta_g & \text{if } \rho_0 \ge 1. \end{cases} \tag{A.2}$$

The values for $\mathcal{P}_{0\ell}$ and $\mathcal{B}_{0\ell}$ are determined by enforcing the continuity conditions at the borehole wall. They are given by

$$\mathcal{P}_{0\ell} = \mathcal{B}_{0\ell} + \mathcal{G}_{0\ell} \qquad \text{and} \qquad \mathcal{B}_{0\ell} = \frac{\mathcal{G}'_{0\ell} - \kappa|\ell|\mathcal{G}_{0\ell}}{(1+\kappa)|\ell|}.$$

For $\ell = 0$, the expression for the latter integration constant is $\mathcal{B}_{00} = 0$. Both $\mathcal{P}_{0\ell}$ and $\mathcal{B}_{0\ell}$ are linear combinations of the specified heat injection rates per unit pipe length, $\mathrm{q}_j(\tau)$, as all involved quantities possess this property.

A.4. Computation of $\mathcal{P}_{jm}$ and $\mathcal{P}'_{jm}$

Finally, the coefficients of the Fourier series expansions around pipe j for Θ_p and its derivative with respect to ρ_j are obtained. To do this, the series defining Θ_p inside the borehole (where $\rho_0 \le 1$) is particularized at the wall of pipe j and split into two parts. After the strategic addition and subtraction of $\mathcal{P}_{00}$, the result is

$$\Theta_p\Big|_{\rho_j=\rho_{pj}} = \sum_{\ell=0}^{\infty}\Big[\mathcal{P}_{0\ell}\big[\rho_0\mathrm{e}^{\imath\theta_0}\big]^{\ell} + \mathcal{P}_{0(-\ell)}\big[\rho_0\mathrm{e}^{-\imath\theta_0}\big]^{\ell}\Big]_{\rho_j=\rho_{pj}} - \mathcal{P}_{00}. \tag{A.3}$$

Next, complex arithmetic is employed to express the position (ρ_0, θ_0) in the polar coordinate system centered at the borehole in terms of the position (ρ_j, θ_j) in the polar coordinate system centered at pipe j:

$$\rho_0\mathrm{e}^{\pm\imath\theta_0} = \rho_{0j}\mathrm{e}^{\pm\imath\theta_{0j}} + \rho_{pj}\mathrm{e}^{\pm\imath\theta_j}.$$

The method for combining these two expressions is demonstrated next using the first series in Eq. (A.3) as an example. After substituting one expression into the other and applying the binomial theorem to the result,

$$\sum_{\ell=0}^{\infty}\mathcal{P}_{0\ell}\big[\rho_0\mathrm{e}^{\imath\theta_0}\big]^{\ell} = \sum_{\ell=0}^{\infty}\mathcal{P}_{0\ell}\sum_{m=0}^{\ell}\binom{\ell}{m}\big[\rho_{0j}\mathrm{e}^{\imath\theta_{0j}}\big]^{\ell-m}\big[\rho_{pj}\mathrm{e}^{\imath\theta_j}\big]^{m}.$$

After carefully inspecting the involved pairs of ℓ and m, it becomes evident that the order of summation can be reversed, resulting in

$$\sum_{\ell=0}^{\infty}\mathcal{P}_{0\ell}\big[\rho_0\mathrm{e}^{\imath\theta_0}\big]^{\ell} = \sum_{m=0}^{\infty}\sum_{\ell=m}^{\infty}\mathcal{P}_{0\ell}\binom{\ell}{m}\big[\rho_{0j}\mathrm{e}^{\imath\theta_{0j}}\big]^{\ell-m}\big[\rho_{pj}\mathrm{e}^{\imath\theta_j}\big]^{m}.$$

Proceeding in the same manner with the second series in Eq. (A.3) allows to rewrite Θ_p particularized at pipe j as follows:

$$\Theta_p\Big|_{\rho_j=\rho_{pj}} = \sum_{m=0}^{\infty}\left[\sum_{\ell=m}^{\infty}\mathcal{P}_{0\ell}\binom{\ell}{m}\big[\rho_{0j}\mathrm{e}^{\imath\theta_{0j}}\big]^{\ell-m}\rho_{pj}^{m}\right]\mathrm{e}^{+\imath m\theta_j} + \sum_{m=0}^{\infty}\left[\sum_{\ell=m}^{\infty}\mathcal{P}_{0(-\ell)}\binom{\ell}{m}\big[\rho_{0j}\mathrm{e}^{-\imath\theta_{0j}}\big]^{\ell-m}\rho_{pj}^{m}\right]\mathrm{e}^{-\imath m\theta_j} - \mathcal{P}_{00}.$$

Now it is straightforward to identify the coefficients $\mathcal{P}_{jm}$ of the Fourier series expansion of Θ_p around pipe j. For $m > 0$, it can be concluded that

$$\mathcal{P}_{jm} = \sum_{\ell=m}^{\infty}\mathcal{P}_{0\ell}\binom{\ell}{m}\big[\rho_{0j}\mathrm{e}^{\imath\theta_{0j}}\big]^{\ell-m}\rho_{pj}^{m},$$

while for $m < 0$ it can be shown that

$$\mathcal{P}_{jm} = \overline{\mathcal{P}}_{j(-m)}.$$

Finally, for $m = 0$ the corresponding coefficient is

$$\mathcal{P}_{j0} = \sum_{\ell=-\infty}^{\infty}\mathcal{P}_{0\ell}\rho_{0j}^{|\ell|}\mathrm{e}^{\imath\ell\theta_{0j}}.$$

The coefficients $\mathcal{P}'_{jm}$ for the Fourier series expansion of the derivative of Θ_p with respect to ρ_j around pipe j are straightforward to obtain:

$$\mathcal{P}'_{jm} = \rho_{pj}\frac{\partial\mathcal{P}_{jm}}{\partial\rho_{pj}} = |m|\mathcal{P}_{jm}.$$

The case $m = 0$, where $\mathcal{P}'_{j0} = 0$, is of particular interest as it is utilized in Sections 4.2 and 4.3 to simplify the formulated systems of linear algebraic equations.

As in all previously presented intermediate steps, the Fourier series coefficients $\mathcal{P}_{jm}$ and $\mathcal{P}'_{jm}$ are linear combinations of the specified heat injection rates per unit pipe length $\mathrm{q}_j(\tau)$. This property is crucial for solving the endogenous first-order problem in Section 4.3.

References

[1] European Union, regulation (EU) 2021/1119 of the European parliament and of the council of 30 June 2021 establishing the framework for achieving climate neutrality and amending regulations (EC) no 401/2009 and (EU) 2018/1999 ('European climate law'), 2021.

[2] International energy agency, 2021, Renewables 2021: Analysis and forecast to 2026.

[3] S. Chen, J. Mao, X. Han, Heat transfer analysis of a vertical ground heat exchanger using numerical simulation and multiple regression model, Energy Build. 129 (2016) 81–91, http://dx.doi.org/10.1016/j.enbuild.2016.07.010.
[4] A.D. Chiasson, S.J. Rees, J.D. Spitler, A preliminary assessment of the effects of groundwater flow on closed-loop ground-source heat pump systems, ASHRAE Trans. 106 (1) (2000) 380–393.
[5] P. Conti, D. Testi, W. Grassi, Transient forced convection from an infinite cylindrical heat source in a saturated Darcian porous medium, Int. J. Heat Mass Transfer 117 (2018) 154–166, http://dx.doi.org/10.1016/j.ijheatmasstransfer.2017.10.012.
[6] R. Fan, Y. Jiang, Y. Yao, D. Shiming, Z. Ma, A study on the performance of a geothermal heat exchanger under coupled heat conduction and groundwater advection, Energy 32 (2017) 2199–2209, http://dx.doi.org/10.1016/j.energy.2007.05.001.
[7] J. Hecht-Méndez, N. Molina-Giraldo, P. Blum, P. Bayer, Evaluating MT3DMS for heat transport simulation of closed geothermal systems, Ground Water 48 (5) (2010) 741–756, http://dx.doi.org/10.1111/j.1745-6584.2010.00678.x.
[8] B. Li, Z. Han, X. Meng, H. Zhang, Study on the influence of the design method of the ground source heat pump system with considering groundwater seepage, Appl. Therm. Eng. 160 (2019) 114016, http://dx.doi.org/10.1016/j.applthermaleng.2019.114016.
[9] Y. Lou, P. fei Fang, X. yu Xie, C.S.A. Chong, F. yuan Li, C. yang Liu, Z. jin Wang, D. yong Zhu, Numerical research on thermal response for geothermal energy pile groups under groundwater flow, Geomech. Energy Environ. 28 (2021) 100257, http://dx.doi.org/10.1016/j.gete.2021.100257.
[10] Y. Nam, R. Ooka, S. Hwang, Development of a numerical model to predict heat exchange rates for a ground-source heat pump system, Energy Build. 40 (12) (2008) 2133–2140, http://dx.doi.org/10.1016/j.enbuild.2008.06.004.
[11] Y. Niibori, Y. Iwata, S. Ichinose, G. Fukaya, Design of the BHP system considering the heat transport of groundwater flow, in: Proceedings of the World Geothermal Congress 2005, Antalya, Turkey, 2005.
[12] J. Raymond, R. Therrien, L. Gosselin, R. Lefebvre, Numerical analysis of thermal response tests with a groundwater flow and heat transfer model, Renew. Energy 36 (1) (2011) 315–324, http://dx.doi.org/10.1016/j.renene.2010.06.044.
[13] J. Bennet, J. Claesson, G. Hellström, Multipole Method to Compute the Conductive Heat Flows to and Between Pipes in a Composite Cylinder, Tech. Rep., Department of Building Technology and Mathematical Physics, Lund Institute of Technology, Lund, Sweden, 1987.
[14] J. Claesson, J. Bennet, Multipole Method to Compute the Conductive Heat Flows to and Between Pipes in a Cylinder, Tech. Rep., Department of Building Technology and Mathematical Physics, Lund Institute of Technology, Lund, Sweden, 1987.
[15] P. Eskilson, Thermal Analysis of Heat Extraction Boreholes (Ph.D. thesis), Department of Mathematical Physics, Lund Institute of Technology, Lund, Sweden, 1987.
[16] P. Eskilson, J. Claesson, Simulation model for thermally interacting heat extraction boreholes, Numer. Heat Transfer 13 (2) (1988) 149–165, http://dx.doi.org/10.1080/10407788808913609.
[17] M. Hermanns, J.M. Pérez, Asymptotic analysis of vertical geothermal boreholes in the limit of slowly varying heat injection rates, SIAM J. Appl. Math. 74 (1) (2014) 60–82, http://dx.doi.org/10.1137/130930170.
[18] P. Cui, W. Yang, W. Zhang, K. Zhu, J.D. Spitler, M. Yu, Advances in ground heat exchangers for space heating and cooling: Review and perspectives, Energy Built Environ. 5 (2) (2024) 255–269, http://dx.doi.org/10.1016/j.enbenv.2022.10.002.
[19] M. Li, A.C.K. Lai, Review of analytical models for heat transfer by vertical ground heat exchangers (GHEs): A perspective of time and space scales, Appl. Energy 151 (2015) 178–191, http://dx.doi.org/10.1016/j.apenergy.2015.04.070.
[20] L. Lamarche, S. Kajl, B. Beauchamp, A review of methods to evaluate borehole thermal resistances in geothermal heat-pump systems, Geothermics 39 (2) (2010) 187–200, http://dx.doi.org/10.1016/j.geothermics.2010.03.003.
[21] K. Nagano, T. Katsura, S. Takeda, Development of a design and performance prediction tool for the ground source heat pump system, Appl. Therm. Eng. 26 (14–15) (2006) 1578–1592, http://dx.doi.org/10.1016/j.applthermaleng.2005.12.003.
[22] M.H. Sharqawy, E.M. Mokheimer, H.M. Badr, Effective pipe-to-borehole thermal resistance for vertical ground heat exchangers, Geothermics 38 (2) (2009) 271–277, http://dx.doi.org/10.1016/j.geothermics.2009.02.001.
[23] A. Chiasson, A. O'Connell, New analytical solution for sizing vertical borehole ground heat exchangers in environments with significant groundwater flow: Parameter estimation from thermal response test data, HVAC & R Res. 17 (6) (2011) 1000–1011, http://dx.doi.org/10.1080/10789669.2011.609926.
[24] Z. Zhao, Y.-F. Lin, A. Stumpf, X. Wang, Assessing impacts of groundwater on geothermal heat exchangers: A review of methodology and modeling, Renew. Energy 190 (2022) 121–147, http://dx.doi.org/10.1016/j.renene.2022.03.089.
[25] J. Claesson, G. Hellström, Analytical studies of the influence of regional groundwater flow by on the performance of borehole heat exchangers, in: 8th International Conference on Thermal Energy Storage, 2000.
[26] M.G. Sutton, D.W. Nutter, R.J. Couvillion, A ground resistance for vertical bore heat exchangers with groundwater flow, J. Energy Res. Technol. 125 (3) (2003) 183–189, http://dx.doi.org/10.1115/1.1591203.
[27] J. Rico, M. Hermanns, Thermal interaction of slender geothermal boreholes with creeping groundwater flows, Appl. Therm. Eng. 236 (C) (2024) 121626, http://dx.doi.org/10.1016/j.applthermaleng.2023.121626.
[28] N. Diao, Q. Li, Z. Fang, Heat transfer in ground heat exchangers with groundwater advection, Int. J. Therm. Sci. 43 (12) (2004) 1203–1211.
[29] N. Molina-Giraldo, P. Blum, K. Zhu, P. Bayer, Z. Fang, A moving finite line source model to simulate borehole heat exchangers with groundwater advection, Int. J. Therm. Sci. 50 (12) (2011) 2506–2513, http://dx.doi.org/10.1016/j.ijthermalsci.2011.06.012.
[30] M. Cimmino, The effects of borehole thermal resistances and fluid flow rate on the g-functions of geothermal bore fields, Int. J. Heat Mass Transfer 91 (2015) 1119–1127, http://dx.doi.org/10.1016/j.ijheatmasstransfer.2015.08.041.
[31] Blocon AB, Earth Energy Designer version 4.20, 2019, https://buildingphysics.com/eed-2/.
[32] U.S. Department of Energy, EnergyPlus version 22.2.0, 2022, Engineering Reference.
[33] P. Eskilson, Superposition borehole model, in: Manual for Computer Code, Department of Mathematical Physics, University of Lund, Lund, Sweden, 1986.
[34] A. Huber, EWS version 5.5: Berechnung von Erdwärmesonden, 2022, Huber Energietechnik AG.
[35] GLHEPro 5.0 for Windows. Users' Guide, School of Mechanical and Aerospace Engineering, Oklahoma State University, 2016.
[36] G. Hellström, Ground Heat Storage: Thermal Analyses of Duct Storage Systems, I. Theory (Ph.D. thesis), Department of Mathematical Physics, Lund Institute of Technology, Lund, Sweden, 1991.
[37] M. Hermanns, New generation of theoretical models for the thermal response of geothermal heat exchangers, IOP Conf. Ser. Earth Environ. Sci. 410 (2020) 012042, http://dx.doi.org/10.1088/1755-1315/410/1/012042.
[38] P.A. Lagerstrom, Matched Asymptotic Expansions: Ideas and Techniques, Springer, New York, 1988.
[39] A. Bejan, Convection Heat Transfer, third ed., Wiley, Hoboken, NJ, 2004.
[40] M. Hermanns, J.M. Rivero, On the quasi-steady limit of the enhanced multipole method for the thermal response of geothermal boreholes, Appl. Therm. Eng. 225 (2023) 120121, http://dx.doi.org/10.1016/j.applthermaleng.2023.120121.
[41] J.M. Rivero, M. Hermanns, Enhanced multipole method for the transient thermal response of slender geothermal boreholes, Int. J. Therm. Sci. 164 (2021) 106531, http://dx.doi.org/10.1016/j.ijthermalsci.2020.106531.
[42] M. Hermanns, S. Ibáñez, Harmonic thermal response of thermally interacting geothermal boreholes, SIAM J. Appl. Math. 80 (1) (2020) 262–288, http://dx.doi.org/10.1137/18M119001X.
[43] S. Cai, X. Li, M. Zhang, J. Fallon, K. Li, T. Cui, An analytical full-scale model to predict thermal response in boreholes with groundwater advection, Appl. Therm. Eng. 168 (2020) 114828, http://dx.doi.org/10.1016/j.applthermaleng.2019.114828.
[44] S. Düber, M. Ziegler, R. Fuentes, Development and validation of a computationally efficient hybrid model for temporal high-resolution simulations of geothermal bore fields, Int. J. Numer. Anal. Methods Geomech. 46 (14) (2022) 2792–2813, http://dx.doi.org/10.1002/nag.3427.
[45] Y. Guo, X. Hu, J. Banks, W. Liu, Considering buried depth in the moving finite line source model for vertical borehole heat exchangers — A new solution, Energy Build. 214 (2020) 109859, http://dx.doi.org/10.1016/j.enbuild.2020.109859.
[46] J. Hecht-Méndez, M. de Paly, M. Beck, P. Bayer, Optimization of energy extraction for vertical closed-loop geothermal systems considering groundwater flow, Energy Convers. Manage. 66 (2013) 1–10, http://dx.doi.org/10.1016/j.enconman.2012.09.019.
[47] J. Hu, An improved analytical model for vertical borehole ground heat exchanger with multiple-layer substrates and groundwater flow, Appl. Energy 202 (2017) 537–549, http://dx.doi.org/10.1016/j.apenergy.2017.05.152.
[48] M. Tye-Gingras, L. Gosselin, Generic ground response functions for ground exchangers in the presence of groundwater flow, Renew. Energy 72 (2014) 354–366, http://dx.doi.org/10.1016/j.renene.2014.07.026.
[49] M. Verdoya, P. Chiozzi, Influence of groundwater flow on the estimation of subsurface thermal parameters, Int. J. Earth Sci. 107 (2018) 137–144, http://dx.doi.org/10.1007/s00531-016-1397-x.
[50] M. Verdoya, C. Pacetti, P. Chiozzi, C. Invernizzi, Thermophysical parameters from laboratory measurements and in-situ tests in borehole heat exchangers, Appl. Therm. Eng. 144 (2018) 711–720, http://dx.doi.org/10.1016/j.applthermaleng.2018.08.039.
[51] C. Wang, X. Wang, J. Lu, Y. Lu, Y. Sun, P. Zhang, A semi-analytical heat transfer model for deep borehole heat exchanger considering groundwater seepage, Int. J. Therm. Sci. 175 (2022) 107465, http://dx.doi.org/10.1016/j.ijthermalsci.2022.107465.
[52] A. Capozza, M.D. Carli, A. Zarrella, Investigations on the influence of aquifers on the ground temperature in ground-source heat pump operation, Appl. Energy 107 (2013) 350–363, http://dx.doi.org/10.1016/j.apenergy.2013.02.043.
[53] S. Erol, M.A. Hashemi, B. François, Analytical solution of discontinuous heat extraction for sustainability and recovery aspects of borehole heat exchangers, Int. J. Therm. Sci. 88 (2015) 47–58, http://dx.doi.org/10.1016/j.ijthermalsci.2014.09.007.

[54] S. Erol, B. François, Multilayer analytical model for vertical ground heat exchanger with groundwater flow, Geothermics 71 (2018) 294–305, http://dx.doi.org/10.1016/j.geothermics.2017.09.008.

[55] T. Metzger, S. Didierjean, D. Maillet, Optimal experimental estimation of thermal dispersion coefficients in porous media, Int. J. Heat Mass Transfer 47 (2004) 3341–3353, http://dx.doi.org/10.1016/j.ijheatmasstransfer.2004.02.024.

[56] J.A. Rivera, P. Blum, P. Bayer, Ground energy balance for borehole heat exchangers: Vertical fluxes, groundwater and storage, Renew. Energy 83 (2015) 1341–1351, http://dx.doi.org/10.1016/j.renene.2015.05.051.

[57] J.A. Rivera, P. Blum, P. Bayer, A finite line source model with Cauchy-type top boundary conditions for simulating near surface effects on borehole heat exchangers, Energy 98 (2016) 50–63, http://dx.doi.org/10.1016/j.energy.2015.12.129.

[58] J.A. Rivera, P. Blum, P. Bayer, Influence of spatially variable ground heat flux on closed-loop geothermal systems: Line source model with nonhomogeneous Cauchy-type top boundary conditions, Appl. Energy 180 (2016) 572–585, http://dx.doi.org/10.1016/j.apenergy.2016.06.074.

[59] Z. Wenke, Z. Linhua, G. Yan, G. Xiang, Z. Hao, Y. Mingzhi, The annual fluctuation of underground temperature response caused by ground heat exchanger in the condition of groundwater seepage, Energy Build. 186 (2019) 37–45, http://dx.doi.org/10.1016/j.enbuild.2019.01.004.

[60] Y. Zhou, Z. xiang Zheng, G. si Zhao, Analytical models for heat transfer around a single ground heat exchanger in the presence of both horizontal and vertical groundwater flow considering a convective boundary condition, Energy 245 (2022) 123159, http://dx.doi.org/10.1016/j.energy.2022.123159.

[61] J. Rico, Impact of Aquifers on the Performance of Geothermal Boreholes for All Peclet Numbers (Ph.D. thesis), Universidad Politécnica de Madrid, Madrid, Spain, 2024.

[62] M. Van Dyke, Perturbation Methods in Fluid Mechanics, annotated ed., The Parabolic Press, 1975.

[63] J. Claesson, G. Hellström, Multipole method to calculate borehole thermal resistances in a borehole heat exchanger, HVAC & R Res. 17 (6) (2011) 895–911, http://dx.doi.org/10.1080/10789669.2011.609927.

[64] W.E. Boyce, R.C. DiPrima, D.B. Meade, Elementary Differential Equations and Boundary Value Problems, 11th ed., Wiley, Hoboken, NJ, 2017.

[65] M. Hermanns, Fast inverse Laplace transform for the unsteady thermal response of geothermal heat exchangers, AIP Conf. Proc. 2186 (1) (2019) 170002, http://dx.doi.org/10.1063/1.5138081.

[66] F.W. Olver, D.W. Lozier, R.F. Boisvert, C.W. Clark (Eds.), NIST Handbook of Mathematical Functions, Cambridge University Press, New York, 2010.

[67] H. Carslaw, J. Jaeger, Conduction of Heat in Solids, second ed., Oxford University Press, Oxford, 1959.

[68] B. Badenes, B. Sanner, M.Á. Mateo Pla, J.M. Cuevas, F. Bartoli, F. Ciardelli, R.M. González, A.N. Ghafar, P. Fontana, L.L. Zuñiga, J.F. Urchueguía, Development of advanced materials guided by numerical simulations to improve performance and cost-efficiency of borehole heat exchangers (BHEs), Energy 201 (2020) 117628, http://dx.doi.org/10.1016/j.energy.2020.117628.

[69] V. Gnielinski, Turbulent heat transfer in annular spaces – a new comprehensive correlation, Heat Transf. Eng. 36 (9) (2015) 787–789, http://dx.doi.org/10.1080/01457632.2015.962953.

[70] J. Rico, M. Hermanns, Modeling the thermal interaction of geothermal boreholes with aquifers using asymptotic expansion techniques, IOP Conf. Ser. Earth Environ. Sci. 588 (5) (2020) 052033, http://dx.doi.org/10.1088/1755-1315/588/5/052033.

[71] M. Hermanns, J.M. Rivero, On the symmetry properties of the network of thermal resistances representing the thermal response of slender geothermal boreholes, Geothermics 94 (2021) 102078, http://dx.doi.org/10.1016/j.geothermics.2021.102078.